



# Verifying QBlade-Ocean: A Hydrodynamic Extension to the Wind Turbine Simulation Tool QBlade

Robert Behrens de Luna<sup>1</sup>, Sebastian Perez-Becker<sup>1</sup>, Joseph Saverin<sup>1</sup>, David Marten<sup>1</sup>, Francesco Papi<sup>2</sup>, Marie-Laure Ducasse<sup>3</sup>, Félicien Bonnefoy<sup>4</sup>, Alessandro Bianchini<sup>2</sup>, and Christian-Oliver Paschereit<sup>1</sup>

<sup>1</sup>Chair of Fluid Dynamics, Hermann Föttinger Institute, Technische Universität Berlin, Müller-Breslau-Straße 8, 10623 Berlin, Germany.

<sup>2</sup>Department of Industrial Engineering, University of Florence, via di Santa Marta 3, 50139 Firenze, Italy.

<sup>3</sup>Saipem - 7 Av. de San Fernando, 78180 Montigny-le-Bretonneux, France.

<sup>4</sup>CNRS – Ecole Centrale Nantes, 1 rue de la Noë 44321 Nantes Cedex 3, France.

**Correspondence:** Robert Behrens de Luna (r.behrensdeluna@tu-berlin.de)

**Abstract.** To realize the projected increase in world-wide demand for floating offshore wind, numerical simulation tools must capture the relevant physics with a high level of detail while being numerically efficient. This allows engineers to have better designs based on more accurate predictions of the design driving loads, potentially enabling an economic breakthrough. The existing generation of offshore wind turbines is reaching a juncture, where traditional approaches, such as the blade element momentum theory and actuator disc models, are becoming inadequate due to the increasing occurrence of substantial blade deflections. QBlade is a tool that includes a higher fidelity aerodynamic model based on lifting-line theory, capable of accurately modeling such scenarios. In order to enable the simulation of offshore conditions in QBlade, and to make use of this aerodynamic capability for novel offshore wind turbine designs, a hydrodynamic module called QBlade-Ocean was developed. In the present work, this module is validated and verified with two experimental campaigns and two state-of-the art simulation frameworks on three distinct floating offshore wind turbine concepts. The results confirm the implementation work and fully verify QBlade as a tool to be applied in offshore wind turbine simulations. Shortcomings reported by comparable tools in the non-linear response to irregular wave excitation are confirmed by QBlade and reiterate the need for further research in this field. A code-to-code comparison with the industry-designed Hexafloat concept highlights the coupled interactions on floating turbines that can lead to large differences in motion and load responses in otherwise identically behaving simulation frameworks.

## 1 Introduction

In recent years, wind turbine technology has seen a dynamic development, characterized by the continuous trend towards increasing tower heights and rotor sizes. This growth has challenged the modeling assumptions of current wind turbine simulation tools. The unfavorable square cube-law scaling that is characteristic to the scaling of blade lengths has already led to innovative slender blade designs which are notably more flexible (Veers et al., 2019). These developments have required wind



turbine simulation tools to move on from the assumption of rigid components and include structural dynamics that enable the analysis of aeroelastic effects and its influence on loads and subsequently designs.

As a consequence, aerodynamic assumptions inherent to the Blade Element Momentum (BEM) method require several corrections to make them viable for modern wind turbines (Perez-Becker et al., 2020; Li et al., 2022). An alternative approach could involve a shift towards physically more accurate models such as a lifting-line coupled with a free vortex wake model. A shift towards higher fidelity aerodynamic methods may be accelerated as wind turbines are placed further offshore, on floating structures that are excited by waves and currents, introducing additional complexity and requiring more accurate models within the wind turbine simulation tools. These capabilities are essential for economic evaluation and optimized engineering solutions of such systems.

To enable economically viable floating offshore wind turbines (FOWTs), simulation tools also require hydrodynamic capabilities to capture the coupled dynamics of aero-hydro-servo-elastic problems and solve the mooring system dynamics. The added degrees of freedom (DoFs) inherent to FOWTs may accelerate the change in how aerodynamic loads and wake aerodynamics are modelled in these increasingly complex scenarios. A floating turbine, unlike its fixed bottom or land-based counterpart, may also interact with its own wake. Modeling this phenomenon accurately, requires resolving the wake explicitly.

At present, FOWTs still rely to a large extent on the BEM method to calculate aerodynamic loads on a wind turbine. This method, while efficient, includes several simplifying assumptions that require empirical corrections. In particular, the rotor is assumed to behave like a planar actuator disk that extracts energy from the stream tube by causing a pressure drop when air flows through it. This assumption inherently omits the finite number of blades on a wind turbine. Moreover, it implies that rotor blades don't deflect outside the rotor plane. Additionally, the momentum theory breaks down for high induction factors and uniform aerodynamic conditions across the rotor plane are assumed (Burton et al., 2001; Perez-Becker et al., 2020; Li et al., 2022). Given the shortcomings of this method and the empirical nature of its corrections, as detailed and explained by Perez-Becker et al. (2020), current BEM methods might not be sufficient in certain circumstances. Ramos-García et al. (2022) analyzed the effects of floating motion on the aerodynamic loads predicted by a BEM and a lifting-line solver. The result of this study was that the BEM method can lead to an increased motion response of up 50% at high wave frequencies. Moreover it was shown that the BEM method underestimates thrust notably during large backwards oscillations, where the turbine interacts with its own wake.

One particular area in which BEM methods need to improve is their modeling of dynamic inflow conditions if they are to maintain their applicability in the future alongside other, more advanced, methods (Jeon et al., 2014). Especially in FOWT modeling, dynamic inflow plays an important role, due to the wave induced motion of the floating structures. Vortex wake models don't have such shortcomings as the wake is modeled explicitly by the trailing and shed vorticity caused by spatial and temporal gradients in the blade-bound vortex. Hence, the wake develops over time and includes the transient effects that, e.g., pitch actuation or gusts have on the induction in the rotor plane (Mancini et al., 2023). The fact that the most recent release of the AeroDyn module (v15) (Murray et al., 2017) of the widely used code OpenFAST (Jonkman et al., 2019) includes a lifting-line aerodynamic method named OLAF (Shaler et al., 2020), may be seen as a confirmation that higher fidelity



55 methods than BEM are a requirement for certain conditions. HAWC2 (Larsen and Hansen (2007)), another well-established state-of-the-art simulation framework, also features multiple aerodynamic solvers based on lifting line theory.

One tool with a numerically-optimized free wake method is QBlade (Marten, 2020). With its hydrodynamic extension QBlade-Ocean, the tool gains the ability to model all required domains to simulate the dynamics of floating wind turbines. Thereby, QBlade addresses a need in the community to provide a numerically efficient code with more accurate aerodynamic and structural models in open access. The development work was carried out within the Horizon2020 project (FLOATECH, 2020) and was identified as a key outcome.

To ensure trust in the results that will be generated with QBlade upon its adoption by the community in the coming years, this work aims to validate and verify the new hydrodynamic extension. This is done on three different floating offshore wind turbine designs. The designs of the floating substructures deviate strongly from each other regarding their stabilization concept, water surface area and structural complexity. These characteristics require modeling approaches appropriate for each design and therefore allow a verification of the various models that are combined to capture the full turbine response to environmental loading. The first FOWT model is the 5MW MARIN Stock Wind Turbine (MSWT) experimental turbine which is mounted on the DeepCwind substructure (Robertson, 2017) and was built and tested thoroughly within the OC5 code collaboration (Robertson et al., 2014). The large number of reference results from the collaboration and the experiments that were carried out make the DeepCwind platform an ideal model to verify and validate the new offshore module of QBlade. Additionally, an equivalent model was built in OpenFAST for reference. The second FOWT that is used for verification purposes is a spar-buoy type platform on which the Softwind Software-in-the-Loop (SIL) experiments focused on (Arnal, 2020). The more complex mooring structure and different stabilization concept compared to the DeepCwind platform make it a suitable choice to continue the validation. As an addition, yet another OpenFAST model was built that serves as a comparison and reference to analyze QBlade's results with respect to the experiment. The third and final model in this work is the Hexafloat concept designed by the company Saipem. This final part documents a code-to-code comparison between QBlade and the industrial software DeepLines Wind<sup>TM</sup> (Principia). DeepLines Wind<sup>TM</sup> was the main tool used during the design process of this substructure. This more complex structure consists of two solid bodies (the hexagon and the counterweight) and provides an opportunity to validate QBlade on a complex platform that was designed with the objective of economic deployment.

80 In Section 2, QBlade and the other simulation tools are presented briefly. Section 3 introduces the models utilized throughout the verification process and highlights the modeling differences between the simulation tools. Section 4 shows the main results of this study and the conclusions are drawn in Sect. 5, which is then followed by an outlook on the intended applications of the fully verified QBlade framework.

## 2 Compared Simulation Frameworks

### 85 2.1 QBlade

QBlade is an openly available simulation tool developed to calculate wind turbine response in the time domain. It has been under development at Technische Universität Berlin (TUB) since 2010, where it started as a coupling between the open-



source panel code XFOIL (Drela, 1989), the graphical user interface (GUI) XFLR5 (Deperrois) and an in-house developed steady BEM solver. The code has been expanded in its capabilities ever since. Today, QBlade features two time domain  
90 aerodynamic solvers. The lower fidelity one is based on the Blade Element Momentum theory. Briefly summarized, the BEM algorithm iterates a set of equations for the tangential and axial induction stemming from the momentum balance and the blade element theory until a converged value for the axial and tangential induction is found. The method has been expanded with several engineering correction methods such as the Prandtl tip loss correction and dynamic inflow filter. The BEM method implemented in QBlade uses a polar grid for the azimuthal discretization of the induction factors, following the approach laid  
95 out by Madsen et al. (2020). In this method, the rotor disc is divided into a polar grid that enables the computation of the local velocity at each intersection taking the local induced velocity and inflow conditions into account. The implementation of the blade element model accurately resolves the velocity at curved stations (e.g. prebend or deflection) by a transformation of the velocity vector into the local coordinate system of the station. The higher fidelity method, the Lifting-Line-Free-Vortex-Wake (LLFW) solver, applies the Lagrangian vortex theory and follows the implementation of van Garrel (2003). The structural  
100 model used in QBlade relies on the finite element analysis (FEA) module of the Project::Chrono multi-physics engine (Tasora et al., 2016). The application in QBlade is such that the structural model of the turbine consists of multiple body objects for the blades and the tower. Each body is modelled as an Euler-Bernoulli beam using a co-rotational formulation with a floating reference frame (Marten, 2020). The total FEA model of a wind turbine is then generated by constraining the different bodies in a multi-body formulation.

105 In the FLOATECH project, QBlade has been extended by a hydrodynamic module that expands its capabilities to offshore conditions. Moreover, the structural model was expanded so that arbitrary substructure geometries can be modeled. Thus, fixed-bottom and floating offshore wind turbines can be designed and analyzed in the simulation suite. More specifically, the hydrodynamic module features:

- 110 1. A wave generator with the capability to generate waves from several energy spectra but also read prescribed wave amplitude time series;
2. A hydrodynamic solver that calculates radiation damping forces, first-order excitation as well as second-order excitation forces (sum and difference frequency) from pre-computed potential flow coefficients;
3. A Morison's equation to account for non-linear drag, added mass and Froude-Krylov forces for arbitrary geometries;
4. A soil model that captures the restoring forces with a distributed spring with non-linear coefficients.

115 Readers interested in more detailed descriptions of the implementation work of QBlade-Ocean are referred to the technical report (Saverin et al., 2021) with the sole focus on methodology and implantation as well as the online documentation (QBlade Documentation, 2022).

The aero-servo-elastic coupling of the LLFW and polar-BEM aerodynamic methods with the structural solver have been validated against different aero-elastic couplings of the simulation tool HAWC2 in Behrens de Luna et al. (2022).



## 120 2.2 OpenFAST

OpenFAST is a widely known open-source multi-physics simulation tool developed by the National Renewable Energy Laboratory (NREL) (Jonkman et al., 2019). OpenFAST builds on a highly modularized framework that couples modules from various physics disciplines with each other to model the behavior of a wind turbine and the environment around it. All OpenFAST results shown in this study were run with OpenFAST v3.0.0. and the BEM solvers implemented in versions v14 (Jonkman  
125 et al.) and v15 (Murray et al., 2017) of the AeroDyn module (depending on the model). The Beddoes-Leishman dynamic stall model and the Øye dynamic wake effects were used. The ElastoDyn module (ElastoDyn) was utilized to resolve the structural dynamics, employing Euler-Bernoulli beam theory with prescribed modes and allowing only edge- and flapwise bending DoFs for the blades, neglecting blade torsion (Rinker et al., 2020). Moreover, the HydroDyn (HydroDyn) module is used to account for the interaction between floater and marine environment. The mooring lines are modeled using MoorDyn (Wendt et al.,  
130 2016).

## 2.3 DeepLines Wind<sup>TM</sup>

DeepLines Wind<sup>TM</sup> (Principia) is a module of the commercial integrated software solution DeepLines<sup>TM</sup> developed by Principia and IFP Energies Nouvelles. It is primarily known as a software solution to calculate in-place and installation analyses for offshore structures such as flexible risers, power cables and mooring systems. Due to the increased market share of wind energy  
135 in the offshore environment, the DeepLines Wind<sup>TM</sup> module was developed in 2011 and is now able to carry out fully coupled dynamic finite element analysis. Multiple BEM models are implemented and can be chosen from an external *.dll* library. Like QBlade, DeepLines Wind<sup>TM</sup> can model horizontal and vertical axis wind turbines. Within this study, a dynamic inflow model was activated while no unsteady blade aerodynamics were applied. A validation study on DeepLines Wind<sup>TM</sup> was carried out by Perdrizet et al. (2013).

## 140 3 Simulation Models and Modeling Approaches

This section briefly introduces the three simulation models used for the validation and verification of QBlade. First, the properties and characteristics of each of the three FOWTs are discussed together with their respective modeling approaches. Second, the areas where the three simulation suites differ from another in the representation of the physics are highlighted and discussed regarding their possible influence on results. Third, the chosen test cases for validation and verification purposes are introduced.  
145 A more extensive description of the three QBlade model definitions can be found in Perez-Becker and Behrens de Luna (2022). Additionally, each turbine database is available on the Zenodo online platform. The corresponding DOIs are provided at the end of this work.

To allow a fair comparison with regard to experimental results (relevant for OC5 and Softwind), each numerical model was tuned independently to match the natural system response of the reference. Details on this matter are specified by Perez-Becker  
150 et al. (2022). Figure 1 displays the three FOWT models with their mooring systems in calm water. The location of the load



sensors consistently used in this work to validate and verify the mooring tensions are labeled in Fig. 2. For the Softwind model, the loads are exported at the delta connector of the mooring system.

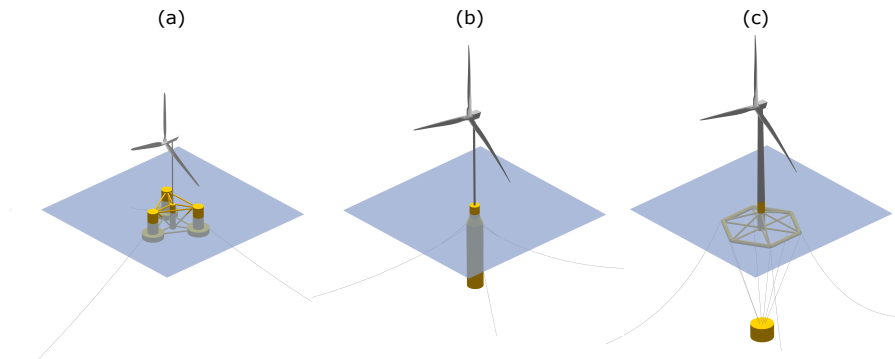


**Figure 1.** Renders of the (a) OC5, (b) Softwind and (c) Hexafloat models exported from the QBlade GUI.

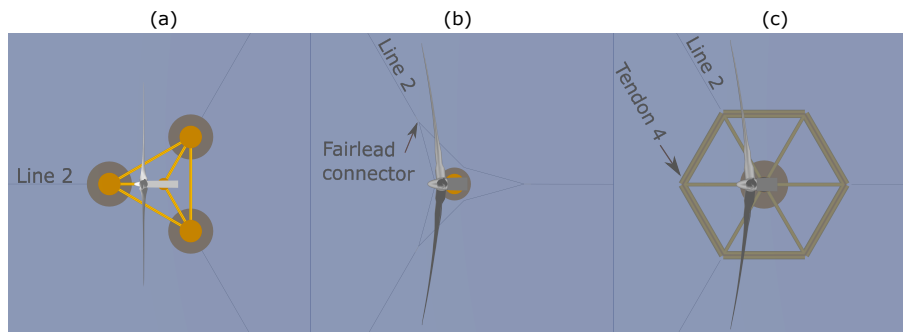


**Figure 2.** Top view of the FOWT models. The incoming wind and wave propagation direction goes from left to right for all considered cases in this study. (a) OC5, (b) Softwind and (c) Hexafloat.

### 3.1 OC5 Model

The first model of a floating offshore wind turbine used for the verification and validation is the MARIN Stock Wind Turbine mounted on the DeepCwind substructure, henceforth referred to as the OC5 model. This FOWT was thoroughly investigated within the Offshore Code Comparison, Collaboration, Continued, with Correlation project (OC5) (Robertson et al., 2014). The OC5 project was operated under the International Energy Agency Wind Task 30 and builds on previous code-to-code comparison efforts (OC3 and OC4). In the OC5 collaboration, a large number of institutions applied various modeling tools with the goal to simulate test cases that were carried out experimentally and relate differences to certain modeling approaches. The experiments were carried out at the Maritime Research Institute Netherlands (MARIN) offshore wave basin. The model on which the experiments were conducted consist of the 1/50<sup>th</sup> scale model of the NREL 5MW RWT turbine mounted on top of the floating semi-submersible substructure. The flexible tower is made out of two aluminium rods that are interconnected



and matches the reference turbine's first fore-aft and side-side natural frequencies. The substructure, as mentioned before, is a three-pillar design semi-submersible known as the DeepCwind platform. It consists of a central column, on which the turbine is mounted, and three additional buoyancy-providing columns that connect to the central column through braces. The scaled platform is moored to the ground with three catenary mooring lines, one attached to each buoyancy column. The QBlade model of the OC5 platform can be seen in Figure 1a. A more precise description of the FOWT is provided by Robertson et al. (2014). Similar to the approach undertaken in the OC5 project, the numerical models are formulated utilizing properties that have been upscaled to match the dimensions of the full-scale size. To compare the numerical results with the experimental ones, the latter too are scaled to full-scale equivalent via Froude-scaling. The OC5 model is particularly well suited for this study as simulation results from a wide variety of simulation codes are openly available for validation purposes and, even more importantly, experimental data can serve as a reference, thus allowing a full validation of QBlade. A comprehensive analysis of the OC5 results is provided by Robertson et al. (2017). Moreover, an equivalent model was built in OpenFAST in order to have full oversight of the subtleties of the model and to have the ability to compare test cases not considered in the OC5 collaboration.

### 3.1.1 OC5 Model - Turbine Modeling Choices

The rotor blades of the model scale NREL 5 MW turbine predominantly consist of MARIN-modified Drela AG04 airfoil sections. The modification was made to reproduce the scaled thrust and torque loads of the reference turbine in a low-Reynolds number environment. The three most inner stations, which amount to roughly 13% of the radius, are blended with a cylindrical airfoil. Due to the minor influence of the root region on aerodynamic performance, the lift coefficient of the inner stations is neglected and an angle-of-attack independent drag coefficient of 0.5 is assigned. Due to the favorable scaling of the structural properties towards full scale, the blades are assumed to be rigid. These choices are in line with the description found in Goupee et al. (2015), where additional information on the MSWT blade, such as chord and twist distribution as well as the modified polars may be found. In both QBlade and OpenFAST, the Øye dynamic stall and the tower shadow models are activated. A tower drag coefficient of 0.5 was used.

### 3.1.2 OC5 Model - Substructure Modeling Choices

The popularity of this DeepCwind substructure within the research community leads to the open availability of hydrodynamic coefficient files that were generated with the boundary element solver WAMIT (WAMIT Inc.). This enables a hydrodynamic treatment that relies on solving the diffraction and radiation problems as well as the calculation of non-linear excitation forces through fully populated sum and difference quadratic transfer functions (QTFs). To account for viscous forces, non-linear drag is resolved via application of Morison drag applied to strip theory, where drag coefficients are assigned to the cylindrical elements. Henceforth, this combination will be referred to as the linear potential flow plus Morison drag (LPMO) approach. The required input files for radiation damping, excitation and second-order wave forces are adopted from the OpenFAST GitHub repository (Jonkman et al., 2019) and are identical for the newly built OpenFAST and QBlade models in this study.



## 195 3.2 Softwind Model

Instead of deploying a scaled physical experimental wind turbine that includes a rotor-nacelle-assembly, as was done in the OC5 campaign, the Softwind experiments rely on a Software-In-the-Loop setup to capture the fully coupled dynamics of a FOWT. The campaign was carried out at the at the Research Laboratory in Hydrodynamics, Energetics and Atmospheric Environment department of the École Centrale de Nantes. The SIL setup includes a digital twin of the Softwind FOWT  
200 that runs in parallel to the experiment and gets information, such as floater displacements and velocities, as an input. The aerodynamics are subsequently solved in the numerical code (OpenFAST), which calculates the rotor's power and thrust force. This information is communicated to a thruster sitting atop the tower, which applies the thrust force of the turbine rotor with close to no time-lag. The FOWT model is scaled to 1/40<sup>th</sup> scale and the turbine is based on the DTU 10MW RWT (Bak et al., 2013) design, appropriately scaled. Accordingly, the RNA mass distribution aligns with the reference wind turbine.  
205 Similarly, the tower properties were scaled down from the DTU 10MW RWT to match the natural frequency of the first fore-aft and side-side modes, the amplitude of deformation and mode shape. The substructure is a spar type foundation which was dimensioned based on existing geometries such as the OC3 Hywind platform (Jonkman, 2010). Finally, the mooring system has been designed with three catenary lines that split up into two lines just before the substructure to form a delta connection for increased yaw stability (see Fig. 2b). The SIL setup and the Softwind model is described more precisely by Arnal (2020).  
210 Figure 1b displays the QBlade model of the Softwind FOWT. Throughout the following sections, this FOWT will be referred to as the Softwind model.

### 3.2.1 Softwind Model - Turbine Modeling Choices

As mentioned in the previous paragraph the rotor of the turbine is, due to the SIL approach, modeled numerically in the experiment as well. Hence, there is no need for re-adjusting the airfoil polars towards a low Reynolds number environment.  
215 Therefore, the blade definition, along with the the airfoil characteristics as outlined in Bak et al. (2013), is utilized to setup the turbine models in QBlade and OpenFAST respectively. In contrast to the OC5 model, this includes the structural definition of the blades and the tower. Both are assumed to be flexible bodies. For servo dynamics, the DTU Baseline Controller (Hansen and Henriksen, 2013) with the corresponding parameters for this turbine was selected. It should be pointed out that the SIL setup included the AeroDyn v14 (Jonkman et al.) module. Hence, the OpenFAST calculations for this turbine also deploy the  
220 AeroDyn v14 module.

### 3.2.2 Softwind Model - Substructure Modeling Choices

The hydrodynamic loads on the spar-type substructure are modeled with the LPMD approach with first order forces relying on potential flow theory. Even though second order forces are generally small in relation to first order forces on spar-buoy type platforms, they can cause notable excitation at the resonant natural frequencies of the platform (Roald et al., 2013). For  
225 this platform, only the main diagonal terms of the difference QTF were available. This in turn yields the opportunity to verify the implementation of Newman's approximation of the slowly varying drift forces within QBlade against experimental results.





Viscous forces are modeled through the application of Morison drag coefficients to the cylindrical elements of the spar. The potential flow coefficients were calculated in a previous step in the open-source software NEMOH (Kurnia and Ducrozet, 2023; Babarit and Delhommeau, 2015) and converted into the WAMIT format.

### 230 3.3 Hexafloat Model

The Hexafloat concept is designed by the company Saipem to provide a cost-efficient substructure with favorable hydrodynamic characteristics. It consists of a hexagonally shaped structure composed of cylindrical members. Twelve braces extend from the six corners inwards, two per corner with varying angles, and converge in a single column. This column is the only member that breaks the water surface in a neutral position and it connects to the tower of the turbine coaxially. The stability of the platform is provided by a counterweight that connects with six tendons to the corners of the hexagonal structure. The QBlade model of the Hexafloat model is displayed in Fig. 1c. Through this design, the benefits of a shallow draft are merged with the characteristics of a spar type floater, including a small water plane area and gravity stabilization. The turbine atop the floater is the DTU 10MW RWT and equals the definition provided by Bak et al. (2013).

#### 3.3.1 Hexafloat Model - Substructure Modeling Choices

240 The Hexafloat structure is modeled with a full-Morison strip theory approach. Accordingly, added mass forces, drag forces and the Froude-Krylov forces are all resolved in an implicit manner using empirical added mass and drag coefficients for the cylindrical elements. This treatment implies that no linear damping is inherent to the system. Diffraction forces are modeled by the application of the MacCamy-Fuchs correction and non-linear hydrodynamic excitation is captured, to some extent, by the application of the hydrodynamic loads at the instantaneous position of the floating structure and by using kinematic wave stretching (Robertson et al., 2017).

### 3.4 Modeling Approaches and Test Cases

Even though QBlade, OpenFAST and DeepLines Wind<sup>TM</sup> are simulation frameworks with similar capabilities on a broader scale, decisions made by the developers regarding the representation of specific physical problems (such as wake induction), can cause smaller scale deviations. In a fully coupled, non-linear system like FOWTs, these deviations may affect overall system dynamics and result in growing deviations throughout the run-time of a full simulation. To help interpret differences in the results between the compared simulation codes, it is important to discuss these modules and their distinctions. Therefore, an overview of the main differences between the three simulation codes is given in the following.

Table 1 summarizes the modeling capabilities of the main physical models of each tool. It can be seen that distinctions are present in various modeling approaches: QBlade deviates from both other codes with its LLFVW method compared to the lower fidelity unsteady BEM approach. Structurally, OpenFAST deviates in the formulation with its ElastoDyn model, which uses a linear model representation that requires the user to provide previously generated mode shapes. QBlade and DeepLines Wind<sup>TM</sup> both use a non-linear beam FEA representation to model the structure of the blades and the tower. Hydrodynamically,



the used OpenFAST version (v3.0.0) is lacking the kinematic stretching option available in QBlade and DeepLines Wind<sup>TM</sup>, possibly showing minor influence on non-linear excitation in the surge and sway degrees of freedom. OpenFAST furthermore  
 260 relies on linear hydrostatics, whereas both other tools compute the buoyancy and restoring forces caused by the displaced water mass explicitly through the submerged volume. Finally, the mooring dynamics are resolved explicitly in each of the three tools, however only QBlade and DeepLines Wind<sup>TM</sup> employ FEA cable elements while OpenFAST follows a lumped-mass approach. Readers interested in greater detail on the modeling formulations are referred to (Marten, 2020; QBlade Documentation, 2022) for QBlade, (Jonkman and Buhl, 2005; OpenFAST Documentation, 2023) for OpenFAST and (Perdrizet et al., 2013) for  
 265 DeepLines Wind<sup>TM</sup>.

**Table 1.** Key differences between the simulation frameworks regarding the respective model.

Model	Code	Aerodynamics	Structure dynamics	Hydrodynamics		Mooring dynamics
OC5 MSWT	QBlade	LLFVW	Non-linear beams	Wheeler stretch	Explicit buoy	Cable elements
	OpenFAST	UBEM	Linear modal	—	Linear buoy	Lumped-mass
SOFTWIND	QBlade	LLFVW	Non-linear beams	Wheeler stretch	Explicit buoy	Cable elements
	OpenFAST	UBEM	Linear modal	—	Linear buoy	Lumped-mass
HEXAFLOAT	QBlade	LLFVW	Non-linear beams	Wheeler stretch	Explicit buoy	Cable elements
	DeepLines Wind <sup>TM</sup>	UBEM	Non-linear beams	Wheeler stretch	Explicit buoy	Cable elements

The authors acknowledge that OpenFAST includes the OLAF solver in its newest AeroDyn v15 release. OLAF is a higher fidelity lifting line solver for aerodynamics similar to the one implemented in QBlade (Shaler et al., 2020). Moreover, OpenFAST includes the BeamDyn structural model that allows for the computation of full geometric non-linearity and large deflections of the blades due to its exact beam theory formulation. The application of both modules was not included in this study. The  
 270 amount of simulations for the different turbine designs was large and the simulations were performed on desktop workstations. Using OLAF and BeamDyn for the OpenFAST calculations would have rendered the evaluation time for these simulations unacceptably large. Finally, NREL released OpenFAST v3.5.0, which includes kinematic wave stretching and explicit buoyancy calculation features, after the underlying simulations for this study were completed.

## 4 Results

275 This section presents the main results of the validation test cases. The test cases selected for this study are intended to validate individual components and models that influence the FOWT dynamics in isolation. Once this initial validation is achieved, the study will move to more complex test cases where all components interact simultaneously. Although not identical, due to the constraint of resembling the experiments, the set of test cases follows a similar approach for each FOWT model:



1. Static cases for assessment of the isolated mooring loads;
  - 280 2. System properties: Decay cases in still conditions for assessment of the natural system properties;
  3. Aerodynamic loads: Wind only cases with with a fixed floater for assessment of the isolated aerodynamic loads;
  4. Hydrodynamic loads: Wave only excitation cases (regular and irregular) for assessment of the isolated hydrodynamics;
  5. Combined aero- and hydrodynamic wind and wave cases for assessment of the combined aero-hydro-servo-elastic dynamics.
- 285 Following this procedure, the results of all three models are discussed and presented for one set of cases before moving to the next set. The respective test cases are defined in tables at the beginning of the associated subsections.

#### 4.1 Static Displacement

The static displacement test cases aim at confirming the static loads caused by the restoring forces of the mooring system which are caused by the displacement of the FOWT model from it's neutral position. In the presented case, the substructure is traversed from positive towards negative surge and sway positions. A close alignment of the results, both with the experiment and other simulation codes, verifies a proper definition of the mooring properties and subsequently, the static loads calculated by the mooring model of QBlade.

290

The static displacement tests were only performed for the OC5 model, since experimental data of these tests was readily available. The mooring tensions on the other models were confirmed in still conditions at the neutral position. The analyzed sensors are the loads at the fairlead positions. For easier visualization, the loads at the fairleads are cumulated to one value in the global surge and sway DoFs and displayed over the displacement displacement direction. Figure 3 shows the results from the OC5 model. The excellent agreement that is displayed by both QBlade and OpenFAST with the experiment, even under significant displacements, allows the conclusion of a correctly defined mooring system and reliable load estimates of QBlade's mooring model in static conditions.

295

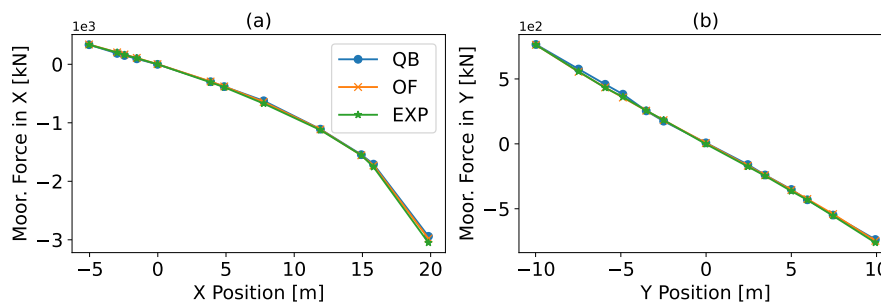


**Figure 3.** Cumulative fairlead loads on the OC5 model obtained from static displacement tests in surge (a) and sway (b). Positive x values indicate a displacement in downwind direction.



## 300 4.2 System Properties - Decay Tests

The dynamic response of a FOWT when it is displaced from its neutral position is affected by several factors, such as system mass and inertia, center of gravity position as well as restoring forces and moments originating from the mooring system and buoyancy. Such decay tests determine the natural frequency and damping of the eigenmodes for the different degrees of freedom. Thereby, these tests are very useful to confirm a correct model setup and give the opportunity to improve alignment of the numerical models with a reference through additional tuning. This subsection presents and discusses the results extracted from the decay time series of the three FOWT models. For more detailed insight, time series and damping characteristics are provided by Perez-Becker and Behrens de Luna (2022) and Perez-Becker et al. (2022).

**Table 2.** Natural frequencies in Hz extracted from the dominant degrees of freedom of each decay time series.

Model	Code	Surge	Sway	Heave	Roll	Pitch	Yaw
OC5	QBlade	0.00944	0.00875	0.05777	0.03083	0.03028	0.01222
	OpenFAST	0.00917	0.00931	0.05777	0.03111	0.03067	0.01208
	Experiment	0.00944	—	—	—	0.03027	—
Softwind	QBlade	0.00844	—	0.03283	—	0.03083	—
	OpenFAST	0.00833	—	0.03250	—	0.03116	—
	Experiment	0.00858	—	0.03264	—	0.03079	—
Hexafloat	QBlade	0.00417	0.00417	0.02694	0.02139	0.02139	0.01750
	DeepLines Wind <sup>TM</sup>	0.00431	0.00430	0.02694	0.02138	0.02138	0.01500

Table 2 shows the natural frequencies as they are extracted from the time series of the decay test for the three FOWT models. The blank spaces indicate that no results of the corresponding test was obtainable. In the case of the OC5 model for instance, the result of the experiment decay test was not publicly available. Thanks to NREL however, the time series of surge and pitch decays were shared upon request. Given that the decay tests of the Softwind model were solely conducted for the surge, heave and pitch DoFs, the numerical simulations were exclusively performed for these corresponding cases. As noted previously for the Hexafloat model, QBlade will only be verified with the commercial software DeepLines Wind<sup>TM</sup> in a code-to-code comparison since for this model no experimental data is available.

By and large, close alignment between the numerical codes and, where available, the experiments has been achieved. Minor deviations can be pointed out for: i) The OC5 model, where OpenFAST deviates with a lower surge natural frequency compared to QBlade and the experiment; ii) The Softwind model, where the same observation also applies. This can be explained through the trade-off that exists between achieving agreement in the fairlead tensions and aligning the surge natural frequency with the experiment. While a slight increase in mooring line stiffness could improve alignment in the surge natural frequency, it influences fairlead tension and might cause a deviation from the desired levels.



### 4.3 Aerodynamic Loads

The next set of test cases considered in this study focuses on isolated aerodynamic excitation. Aerodynamic loads affect the dynamics of FOWTs through changes in rotor thrust. This can lead to strong excitation in the substructure surge and pitch DoFs. The test cases follow the setup defined in the first two aerodynamic cases of the OC5 phase II collaboration (Robertson et al., 2014) to be able to compare to the experimental reference model. This was done for two different rotors: the one used in the OC5 experiment and the DTU 10 MW RWT rotor, used on the Softwind and Hexafloat models, respectively. For the OC5 model, two rotor characteristic curves are recorded with an rotor speed sweep over the same wind field. One representing close to rated and the other one above-rated conditions of the OC5 turbine model. The substructure meanwhile is constrained at its neutral position and hence doesn't respond dynamically to the excitation. The second rotor that was tested is the one from the DTU 10 MW RWT. The Softwind experiment, following a SIL setup, applies the aerodynamic loads that are calculated in real-time along the experiment by AeroDyn v14. Accordingly, a verification with OpenFAST using AeroDyn v14 assures alignment with the experiment. Since DeepLines Wind<sup>TM</sup> is used in the Hexafloat code-to-code comparison, it is included in this test case. To isolate aerodynamic loads, the comparison was carried out on a simplified geometry of the DTU 10 MW turbine that has a rigid tower, no shaft tilt and also no coning angle. The shape of the blades and their flexibility was not modified. The aerodynamic thruster installed in the SIL experiments only applies the thrust force at a single point on top of the tower. Hence, for this turbine, the thrust coefficient was the main point in the comparison. In each software package, the thrust force applied on the rotor shaft was used to calculate the thrust coefficient. A description of the test cases can be found in Table 3.

**Table 3.** Description of test cases 2.1 and 2.2. Isolated aerodynamic excitation with a constrained substructure at its neutral position.

Test case	Turbine	Rotor speed [ $\text{min}^{-1}$ ]	Blade pitch $\beta$ [deg]	wind speed [m/s]	turbulence	Length [min]
2.1	OC5 MSWT	5.5 - 17.0	$0.86^\circ$	12.91	5%	20
2.1	DTU 10 MW RWT	3.0 - 13.0	$0^\circ$	8	0%	until converged
2.2	OC5 MSWT	5.5 - 17.0	$15^\circ$	21.19	5%	20
2.2	DTU 10 MW RWT	2.5 - 9.0	$15^\circ$	15	0%	until converged

The average value for  $C_p$  and  $C_t$  for each rotor speed of the OC5 turbine sweep is displayed in Fig. 4. The reference results that are displayed stem from the study of Goupee et al. (2015), in which the polars of an OpenFAST model were calibrated to resemble the aerodynamic behavior of the OC5 turbine. Two curves can be seen for each coefficient. Test case 2.1 ranges from a tip speed ratio (TSR) of 2.8 up to close to 9 and represents a rotor speed-sweep at constant, close to rated, wind speed with  $0.89^\circ$  pitch angle. Test case 2.2 ranges from a TSR of 1.7 up to 5.3 at wind speeds representing above-rated condition. Focusing on the power coefficient first, little deviation between both numerical tools is visible even though different aerodynamic models are deployed. Bearing in mind that the blades of the OC5 turbine are modeled as rigid structures and are almost perfectly straight, the planar rotor assumption underlying the BEM method are not violated. Hence, good alignment is to be expected.



Small deviations from the experiment are visible above a TSR of 6.5, which is in alignment with Goupee et al. (2015). As he states, this is probably a side effect caused by the primary objective during the polar tuning process, which was carried with the objective to match the experiment's thrust behavior. The turbine's operating point during the experiment will be just below  
 350 TSR 6, where good agreement is present between the both codes and the experiment. The thrust coefficient shows excellent agreement between QBlade, OpenFAST and the experiment.

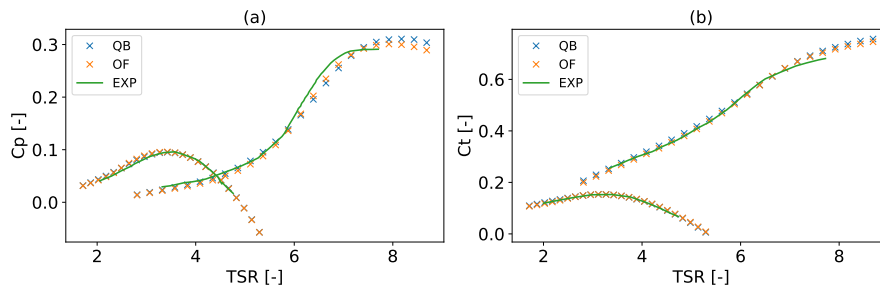


**Figure 4.** OC5 turbine power (a) and thrust (b) coefficients for test case 2.1 - at lower TSRs and test case 2.2 - at higher TSRs.

Figure 5 shows the thrust coefficient for two rotor speed sweeps at just below-rated condition (test case 2.1, Fig.5a) and well above (test case 2.2, Fig.5b). Inspecting the below-rated case first, it can be seen that for lower TSRs, close agreement between the numerical codes exists. In the region above a TSR of 10, which is representative of cut-in and below-rated conditions,  
 355 DeepLines Wind<sup>TM</sup> shows increasing deviation from OpenFAST and QBlade. The latter two continue to show good agreement in that region. At and below-rated conditions (TSR = 8), excellent agreement is present between all codes. In the second sweep, where blades are collectively pitched to 15° and above-rated wind speeds are present, DeepLines Wind<sup>TM</sup> underpredicts thrust compared to QBlade and OpenFAST in the TSR range between 3 and 5. Below this region, good agreement is achieved. The conditions analyzed later in this paper will resemble states at around TSR equal to 8 in test case 2.1 and TSR equal to 6 in test case 2.2. In both, acceptable agreement is found in steady conditions.

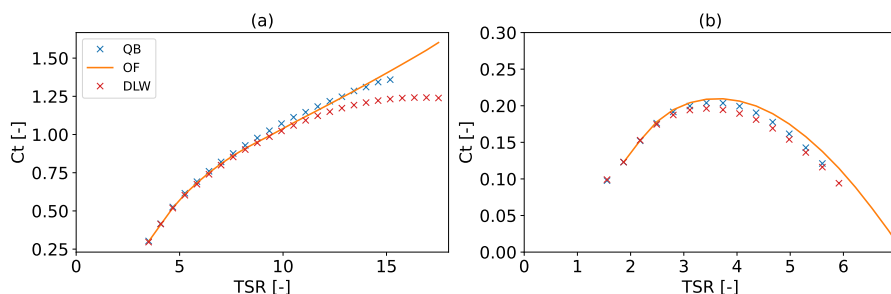


**Figure 5.** DTU 10 MW RWT thrust coefficients for test case 2.1 (a) and test case 2.2 (b).



## 4.4 Hydrodynamic Loads

**Table 4.** Test cases 3.1 and 3.2 description. Isolated hydrodynamic excitation applied to the free-floating substructure without aerodynamic loads.

Test case	Model	Wave condition	Wave characteristics	Length [min]
3.1	OC5	Regular Wave	H = 9.41 m, T = 14.3 s	20
3.1	Softwind	Regular Wave	H = 9 m, T = 18 s	5
3.1	Hexafloat	Regular Wave	H = 9 m, T = 18 s	10
3.2	OC5	Irregular Wave	Hs = 7.1 m, Tp = 12.1 s, JONSWAP	176
3.2	Softwind	Irregular Wave	Hs = 9.4 m, Tp = 14 s, JONSWAP	60
3.2	Hexafloat	Irregular Wave	Hs = 9.4 m, Tp = 14 s, JONSWAP	20

The isolated hydrodynamic (wave-only) test cases considered in the following amount to one regular wave and one irregular wave case for each of the models. After the confirmation of the mooring loads and the systems decaying behavior (see Sect. 4.1 and Sect. 4.2), the excitation by solely hydrodynamic loads without considering aerodynamic effects allows the validation of the hydrodynamic loads computed by QBlade. Thanks to the distinct nature of the hydrodynamic modeling characteristics of the three models, i.e., LPMD for OC5 and Softwind and full Morison for Hexafloat, the implementation of hydrodynamic theory in QBlade can be validated in a general sense. When using the LPMD approach in regular wave test cases, the first order excitation forces calculated via excitation force coefficients are driving the floater response. In the full Morison case, the wave excitation is captured by the instantaneous wave elevation (Froude-Krylov force) combined with diffraction effects captured with the MacCamy-Fuchs correction. In an irregular wave field, the floater response to the linear wave excitation spectrum is validated. In this subsection, our main focus is to validate the linear response along with non-linear excitation due to slowly varying drift forces (OC5 and Softwind), the application of hydrodynamic loads at the instantaneous position (Hexafloat) and the kinematic wave stretching (all models). A detailed description of the test cases can be found in Table 4.

### 4.4.1 Regular Wave Excitation

Figure 6 displays the response amplitude operators (RAOs) of the OC5, Softwind and Hexafloat FOWTs in the three mainly excited motion DoFs. The RAO provides a quantitative value of the FOWT's response under regular wave excitation. It can be understood as a transfer function that quantifies the motion response for a given excitation. As is done by Robertson et al. (2017), the RAO is defined as the ratio of the amplitude of the rigid body motion to the amplitude of the wave frequency. RAOs are effective in validating the linear wave-induced excitation of the model, which is the objective of this section. Across the three models, excellent agreement is present. QBlade demonstrates good agreement with the experiments and OpenFAST in case for the OC5 and Softwind platforms (Fig. 6a and b). When compared to the large database from the OC5 collaboration,



QBlade falls in line with the superior performing simulation codes (Robertson et al., 2017). For the Hexafloat model, good agreement with DeepLines Wind<sup>TM</sup> is found (Fig. 6c).

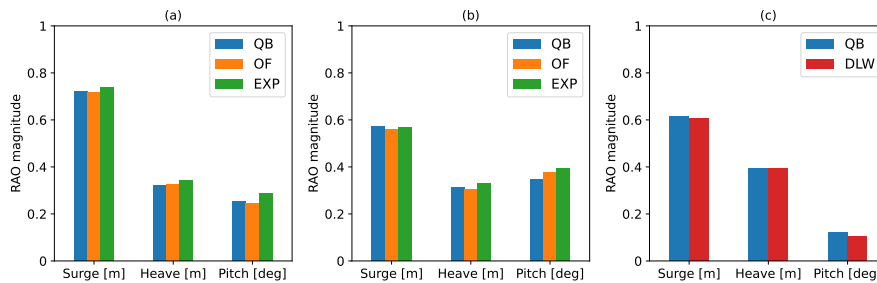


**Figure 6.** RAOs extracted from the time series corresponding to TC 3.1 for the (a) OC5, (b) Softwind and (c) Hexafloat models.

Since floating offshore wind turbines are coupled systems, non-linear responses may occur even under regular wave excitation. Especially, as we compare to experimental setups that can only approximate an ideal regular wave which contains only a single frequency component. Hence, in addition to the RAOs, we analyze the time series of several load sensors of the OC5 model in Fig. 7. The tower top force and the tower base moment in fore-aft direction indeed show a more irregular pattern compared to the fairlead tensions and platform surge motions. This effect can be explained by the fact that the basin boundaries lead to the existence of multiple wave components (e.g. through reflection), which result in a wave field that includes more components than the excitation frequency. This phenomenon is captured in the numerical codes since the time series of the experiment is used as a direct input. Figure 8 reinforces this thesis by showing the power spectral density (PSD) of the corresponding quantities. The multiple peaks of the wave power spectrum can clearly be seen, causing an excitation in the tower responses at its natural frequency of approximately 0.31 Hz. QBlade captures this coupling between wave excitation and tower structure well and aligns with the experimental results and OpenFAST.

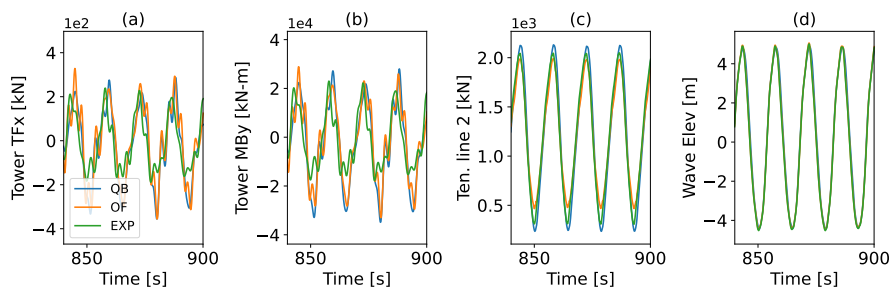


**Figure 7.** OC5 model response to TC 3.1 - regular wave excitation in (a) tower top force in x, (b) tower base fore-aft moment, (c) fairlead tension line 2 and (d) wave elevation.



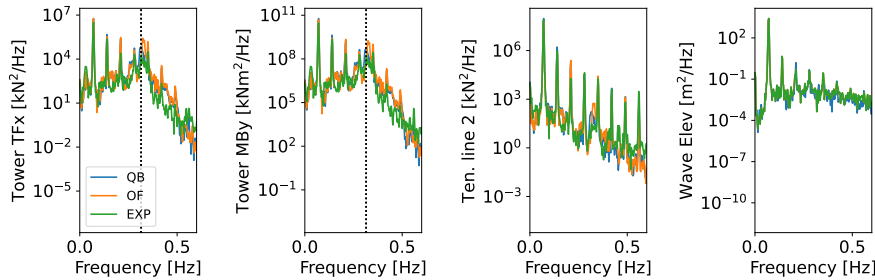


**Figure 8.** OC5 model PSD corresponding to TC 3.1 - regular wave excitation in (a) tower top force in x, (b) tower base fore-aft moment, (c) fairlead tension line 2 and (d) wave elevation. Black dotted line highlights the first tower fore-aft natural frequency.

395 Figure 9 shows the PSDs of equivalent sensors from the Softwind model. Since the time series results from this model provides only limited additional information to the OC5 results, further data is not shown for brevity. It stands out that in this experimental campaign, in addition to the dominant frequency at 0.055 Hz, there are less pronounced peaks at higher order harmonics in the PSD of the wave elevation. Accordingly, the excitation of the tower fore-aft mode is considerably smaller which is reflected in the tower base moment sensor (Fig. 9a). The QBlade result is in agreement with this point and shows good alignment with the experimental results and OpenFAST. The distinct peaks in the spectrum of the tension of mooring line 2, most prominently the one at the wave excitation frequency, are all captured accurately by QBlade.

400

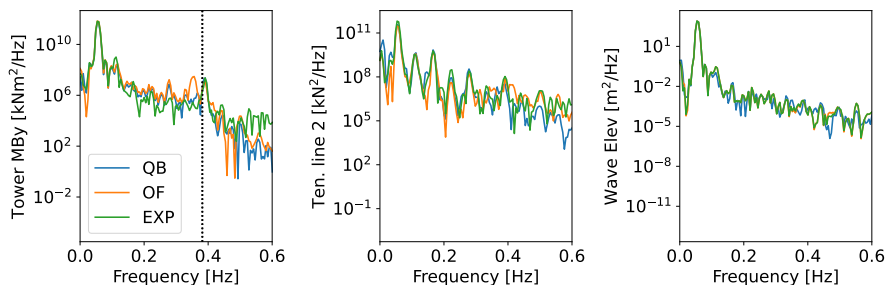


**Figure 9.** Softwind model PSD of selected load sensors from test case 3.1 - regular wave excitation in (a) tower base fore-aft moment, (b) fairlead tension line 2 and (c) wave elevation. Black dotted line highlights the first tower fore-aft natural frequency.

To conclude test case 3.1, the time series of selected sensors for the Hexafloat model are displayed in Fig. 10. They confirm the good alignment indicated by the RAO. A modest increase in tower base moment in fore-aft direction is visible in the amplitude of the QBlade result. A presumable cause is the slightly increased pitch RAO (see Fig. 6c). The tension in line 2, which spans diagonally in negative x-direction (contrary to wave propagation) and positive y-direction as highlighted in Fig. 2c, displays a disagreement regarding the mean tension of approximately 1.5% between both codes. The last two sensors (Fig. 10c and d) aim at capturing the counterweight dynamics via one of the tendons that connects the counterweight to the floating substructure and the counterweight's CoG-surge displacement (see Fig. 2c). Excellent agreement in both cases can be observed.

405



For this comparison, the wave field is generated in both codes with Airy wave theory. Given the perfectly monochromatic nature  
410 of the wave input and the similarly monochromatic load response, the analysis of the response in the frequency domain is left  
out for brevity.

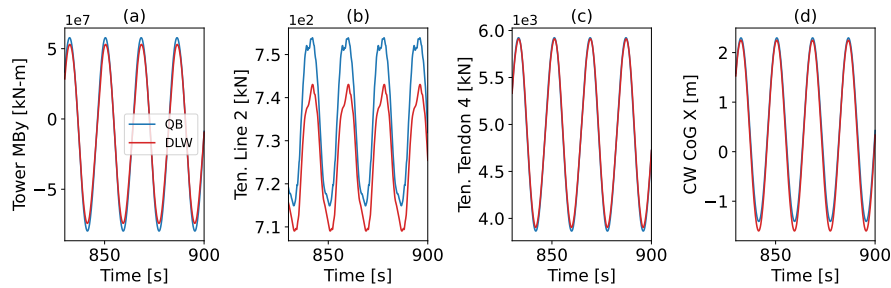


**Figure 10.** Hexafloat model response to TC 3.1 - regular wave excitation in (a) tower base fore-aft moment, (b) fairlead tension line 2, (c) tension in tendon 4 and (d) wave elevation.

#### 4.4.2 Irregular Wave Excitation

Continuing with the isolated hydrodynamic excitation cases, the complexity is increased by considering excitation from irregular wave spectra in this subsection. Figure 11 displays the two load-driving motion DoFs (surge and pitch) next to the  
415 fore-aft tower base moment and fairlead tension of line 2. As for the regular wave case, good visual agreement is present in the motion time series, especially between both numerical codes. The experiment shows differences mainly in the surge and, to a lesser extend, in the pitch DoF. Both seem to contain a low-frequency component in the experimental result which is not well captured by the numerical tools. One full period of this low frequency is evident in the surge subfigure between approximately 750 s and 850 s (Fig. 11a). This period matches the surge natural frequency of the floater with approximately 0.01 Hz (See  
420 Table 2). The fore-aft tower base moment demonstrates a higher frequency component caused by an excitation of the tower eigenmode. Here, larger deviations to the experiment become obvious and will be analyzed in more detail in the frequency domain. Beside higher frequencies in the tower response, the wave excitation frequency can be made out and displays good alignment between QBlade, OpenFAST and the experiment. The tension in fairlead 2 correlates closely with the surge motion, given that it provides the main restoring force. Interestingly, the slow surge frequency, which is only seen in the experimental  
425 response, translates to the fairlead tension in a much reduced manner.

The evaluation of the full test case on a statistical basis is presented in Fig. 12, where the PSD of selected sensors along with their distribution visualized with box-whisker plots is displayed. The PSD can be categorized into several regions: linear wave excitation between 0.05 Hz and 0.3 Hz, the platform's natural frequencies in surge (0.01 Hz) and pitch (0.03 Hz) below the wave frequency range and the tower natural frequency at about 0.32-0.34 Hz. Focusing on the platform motions first, QBlade  
430 shows excellent agreement with the reference results from the experiment and agrees with OpenFAST regarding the linear wave excitation frequencies. Below the wave frequency spectrum, peaks in the natural frequency of each motion DoF are

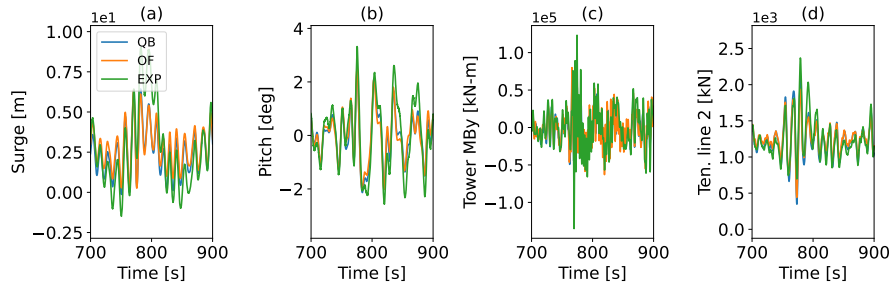


**Figure 11.** OC5 model response to TC 3.2 - irregular wave excitation in (a) surge, (b) pitch, (c) tower base fore-aft moment and (d) fairlead tension line 2 .

visible. Within these frequencies, QBlade predicts modestly more energy compared to OpenFAST. The experimental results in contrast, show a much higher energy within the natural frequencies of surge DoF and, to a lesser extent, the pitch DoF. This phenomenon was noticed in the OC5 collaboration (Robertson et al., 2017) and subsequent analyses in phases Ia and Ib of the OC6 project (Robertson, 2019). It was found that the inclusion of second order difference frequency forces led to a response at the accurate frequency. However, excitation at these low frequencies is smaller when compared to experimental results. Studies focusing on this matter indicate that the addition of linear damping and stiffness coefficients during the tuning process restrict the response. A detailed analysis is given by (Robertson et al., 2020; Robertson and Wang, 2021). QBlade, in contrast to OpenFAST, includes Wheeler stretching which causes a minor improvement in the response of its surge natural frequency. In the pitch DoF, both numerical codes show almost identical energy spectra, underestimating the response in the pitch natural frequency. This underestimation of low frequency response is visible in the load sensors as well. The tower bottom and fairlead load PSDs both show a reduced response in the pitch (tower base) or surge (fairlead 2) natural frequencies compared to the experiment. Above the linear wave excitation frequency the natural fore-aft frequency of the tower is evident in the tower base moment PSD. Here, the different structural representation of the tower between QBlade and OpenFAST comes to bear. Even though both tools predict similar natural frequencies (Perez-Becker et al., 2022), the shape of the peak is resembled more closely in OpenFAST while the excitation frequency itself is matched better by QBlade.

For a statistical evaluation of the data, the platform motions and load sensors are shown in box-plots in the second row of Fig. 12. Box-plots categorize the data in five quantities, the 1- and 99 percentile thresholds (outer whiskers), the first and third quartiles (height of the box) and the median (black line inside the box). Outside the whiskers lie flier values that are considered extreme outliers. At first, the platform motion is analyzed. The surge and pitch interquartile ranges (IQRs) predicted by QBlade amount to a decrease of 28% and 22%, respectively, compared to the experiment. This is an improvement compared to the respective OpenFAST values of -32% in surge and -23% in pitch (Figs. 12a and b). The median position of the experiment is matched more closely by OpenFAST in surge and by QBlade in pitch. As was noted throughout the different test cases, both numerical tools did not capture certain frequency responses that were visible in the experimental data; mainly in surge but also in the pitch degree of freedom. This low frequency component most likely leads to the larger IQR and spread of



whiskers in the corresponding experimental box-plot and to a more skewed distribution of the displacements in surge. With regards to the tower loads and fairlead tension, few systemic distinctions can be identified indicating a similar distribution and good alignment of data from QBlade, OpenFAST and the experiment.

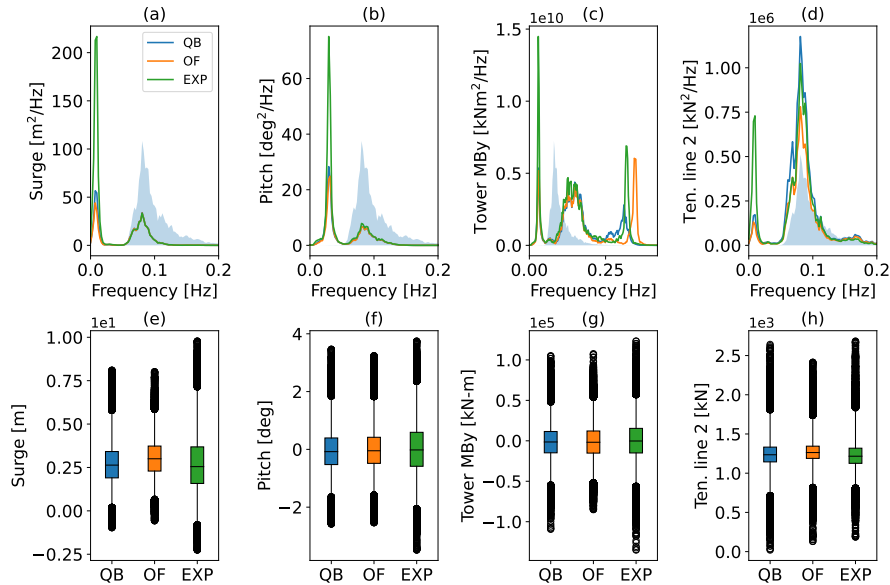


**Figure 12.** OC5 model response to TC 3.2 - irregular wave excitation. PSD of (a) surge motion, (b) pitch motion, (c) tower base fore-aft moment and (d) fairlead tension line 2 and the corresponding box-whisker plots (e) - (h). The qualitative wave spectrum is displayed with transparent blue color in the background for reference.

To facilitate a more focused discussion, the time series data of the Softwind model is omitted, as only very limited additional insight is contained. The main observations are similar to the ones seen in Fig. 11, with more pronounced long period responses in the surge and pitch DoFs, that translate into the response of the tower and mooring load sensors. As will be shown in the box-plot analysis, an offset in mooring loads was present that amounts to approximately 8% difference in mean tension.

In Fig. 13, the Softwind model response to an equivalent test case is analyzed with the same quantitative methods. In the surge PSD (Fig. 13a), the response within the linear wave spectrum is equivalent between the three results. In the peak of the surge natural frequency, the formerly seen shortcoming regarding non-linear excitation is also visible in both simulation codes on this spar-type FOWT. QBlade and OpenFAST demonstrate equivalent energy within this frequency, indicating that Newman's approximation implemented in QBlade, performs similarly to the implementation in OpenFAST. Furthermore, it implies a lesser influence of kinematic stretching on this model. The corresponding box-plot confirms this with no deviation in the IQR between QBlade and OpenFAST. Both tools underpredict the IQR in surge by 29% (Fig. 13e). Again, the increased non-linear response seen in the experiment PSD is the presumable cause. The median value is shifted slightly as a result of different neutral positions in both numerical tools with respect to the experiment. The pitch DoF (Fig. 13b) shows an increased response

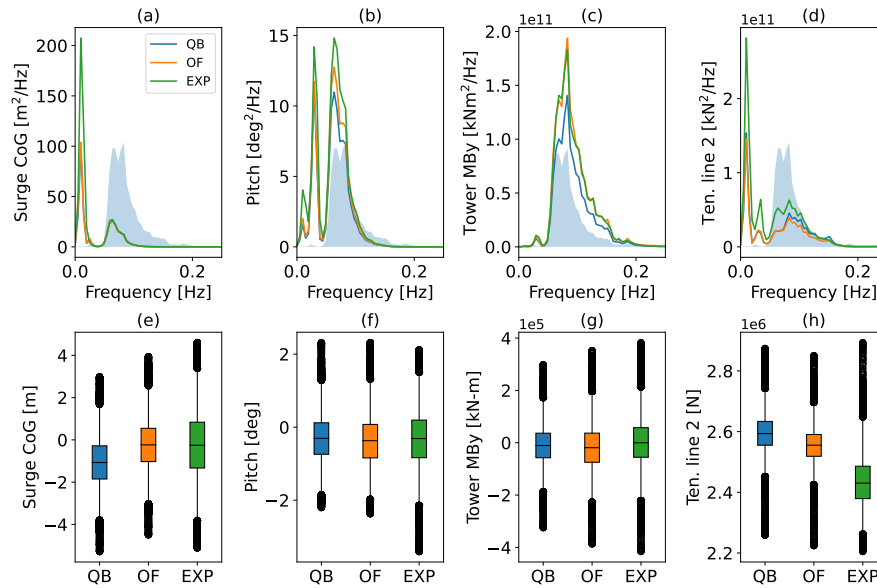


**Figure 13.** Softwind model response to TC 3.2 - irregular wave excitation. PSD of (a) surge motion, (b) pitch motion, (c) tower base fore-aft moment, (d) fairlead tension line 2 and the corresponding box-whisker plots (e) - (h). The qualitative wave spectrum is displayed with transparent blue color in the background for reference.

within the linear frequency range in the experiment. Here, OpenFAST displays closer agreement to the reference compared to QBlade. This could be caused by deviation in the mooring loads between the tools that results in a more constrained response in the pitch DoF in QBlade (Fig. 13h). However, it should be noted that the amplitudes are small and therefore small absolute deviations - in the order of a tenth of a degree - causes this relatively large appearing deviation seen in the PSD.

475 The non-linear excitation paints a similar picture when compared to the OC5 results, with QBlade and OpenFAST accurately determining the frequency, but with a decrease in amplitude. The box-plot (Fig. 13f) demonstrates good alignment among the compared instances and highlights the occurrence of generally minor amplitudes in the pitch response. QBlade and OpenFAST underestimate the IQR by 16% and 10% respectively. The tower base loads (Figs. 13c and g) reproduce observations from the

480 pitch PSD to some degree, albeit with different relative magnitudes between the non-linear and the linear frequency response range, with the former barely visible. Again, close agreement prevails in the box-plot with similar distribution of data between the 1- and the 99-percentiles between the compared results. Finally, the tension in fairlead 2 (Figs. 13d and h) also shows a considerable response in the non-linear surge natural frequency, directly related to the increased surge response noted in the

485 experiment. Additionally, the increased response within the linear frequency range that is visible in the experiment's PSD is not fully reproduced by the numerical tools. The lower mooring tension in the experiment allows for larger amplitudes in the system. QBlade overestimates the median tension by 6.3% and OpenFAST by 5%. The skewed value distribution compared to QBlade and OpenFAST is likely a consequence of this.

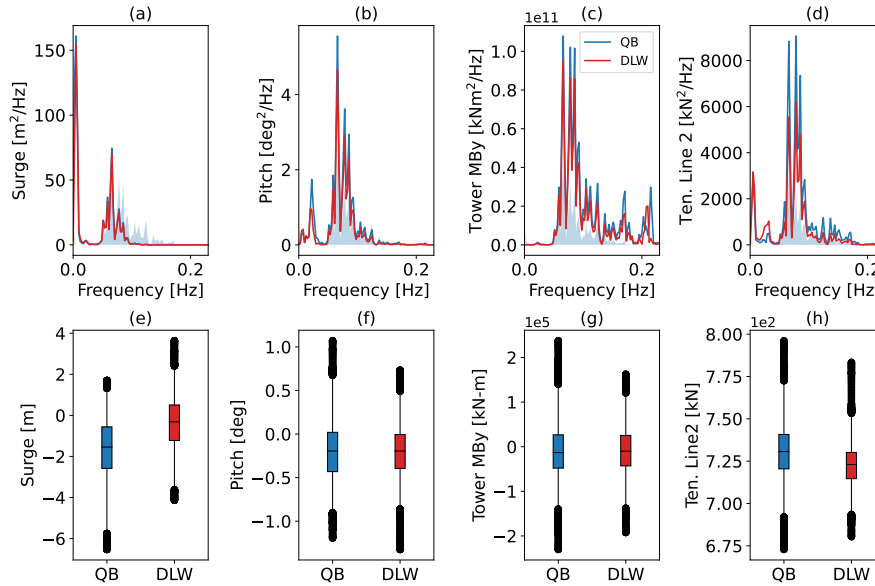


**Figure 14.** Hexafloat model response to TC 3.2 - irregular wave excitation. PSD of (a) surge motion, (b) pitch motion, (c) tower base fore-aft moment, (d) fairlead tension line 2 and the corresponding box-whisker plots (e) - (h). The qualitative wave spectrum is displayed with transparent blue color in the background for reference.

To conclude the isolated wave excitation test cases, the Hexafloat model is analyzed. As for the Softwind model, the time series result is only briefly summarized. The motion sensors demonstrate very close alignment with regard to the dynamic response. A mean offset in the surge position of approximately 0.75 m upstream is visible in QBlade that can be accredited to minor differences in the mooring tension. Notably, the amplitudes of the pitch motion were slightly increased in QBlade which causes a minor increase in the tower base moment response as a result.

Figure 14 illustrates a high degree of similarity between the responses of tools in both degrees of freedom within the linear excitation frequency range of the wave spectrum, as well as in the non-linear response within the surge and pitch natural frequencies below the wave spectrum (Figs.14a and b). Notably, no QTFs were available for this model, providing the opportunity to validate the weak, non-linear excitation caused by the application of hydrodynamic loads at the instantaneous floater position combined with kinematic stretching. Both, the tower fore-aft moment and fairlead tension in line 2 show good agreement in the excited frequencies, with QBlade predicting moderately higher peaks at the relevant frequencies (Figs. 14c and d). This can be attributed to a slightly larger surge and pitch response within the linear wave spectrum, visible in the corresponding PSDs. The box-plot results show the effect of the increased response throughout the linear frequency range in QBlade: In surge, the IQR is 14% larger in QBlade while the median is shifted in negative x-direction (Figs.14e). The platform pitch and tower base moment data are in good agreement with regards to their median value. Their IQR range is again larger in QBlade (Figs.14f and g) with 19% increased spread in pitch that translates to a 10% increase in the tower base moment spread.



Finally, the box-plot of the tension in line 2 (Fig. 14h) displays a mirrored pattern compared to the surge box-plot, indicating  
505 their close dependency. QBlade predicts a 30% larger IQR compared to DeepLines Wind<sup>TM</sup>.

#### 4.5 Combined Aero- and Hydrodynamic Loads

The final test case, which concludes this verification and validation study, combines the fully coupled aero-servo-hydro-elastic  
dynamics exhibited by a floating offshore wind turbine throughout its lifetime. As before, we perform qualitative analysis of  
cut-out time series for one exemplary model, in this case the Softwind model, at the beginning of this section. Subsequently,  
510 quantitative statistics are used for each model to assess the predicted responses by QBlade, and to compare them to the nu-  
merical counterparts and experimental reference cases. Table 5 showcases the three test cases considered, one for each FOWT  
assembly. To cover three different operational states, varied environmental conditions are selected for each FOWT. The Soft-  
wind model is simulated in conditions beyond the rated regime, where the controller constantly actuates the blade pitch to not  
exceed rated power output. Conversely, the simulation of the OC5 model approximates conditions that are near to rated power.  
515 This is done with a constant prescribed value for the blade pitch angle and rotor speed (as was done in the OC5 collaboration).  
In case of the Hexafloat model, below-rated conditions are discussed. Here, the controller gradually adjusts the rotational speed  
to operate at the optimal tip speed ratio to maximize power generation. For the servo control of the DTU 10 MW turbine atop  
the Softwind platform, the DTU Baseline Controller (Hansen and Henriksen, 2013) is used, again, replicating conditions from  
the experiment. The control parameters correspond to those of the reference turbine except for the proportional and integral  
520 gains of the pitch controller and the linear and quadratic aerodynamic gain scheduling coefficients, which were adjusted to  
prevent negative damping that originates from the coupling between blade pitch actuation and the floater pitching motion. The  
PI parameters of the OO-Star 10 MW FWT are used, since the pitch natural frequency between both the OO-Star and Softwind  
platforms is nearly identical (Yu et al., 2018). In case of the Hexafloat model, the ROSCO v 2.4.1 controller (NREL, 2021)  
was selected due to its ability to include a velocity feedback damping loop designed to reduce pitching motion and thereby  
525 increase stability of the floating substructure. Unfortunately, this feature had to be disabled for this code-to-code comparison  
after difficulties were found in the communication between the ROSCO controller and DeepLines Wind<sup>TM</sup>. Leaving this fea-  
ture active in QBlade alone would have impeded a consistent comparison. Therefore, the controller gains were de-rated to  
prevent negative damping effects instead.

The Softwind model is analyzed at above-rated conditions, with a mean wind speed of 18 m/s that requires continuous blade  
530 pitch actuation by the DTU wind turbine controller. The blade pitch actuation is based on the power output of the wind turbine,  
which depends on the velocity in the rotor plane. Hence, blade pitch actuation depends on the motion induced velocities and  
the wake-induced velocities in the rotor plane of the system. Considering this, the wake model (lifting-line vs. BEM) and the  
hydrodynamic model (buoyancy modeling, wave kinematics) in a given simulation collectively influence the pitch actuation  
process and subsequently the overall system dynamics. Figure 15 shows a cut-out of the time series displaying the same  
535 sensors that were chosen in TC 3.2 to analyze the system response of the Softwind model. What stands out is that even after  
more than ten minutes into the time series, good qualitative agreement between the three compared results is present. The  
surge time trace demonstrates a long period cycle at the natural frequency of this degree of freedom. OpenFAST demonstrates

**Table 5.** Test case 4.1 description. Combined aero-hydrodynamic-servo-dynamic conditions applied to the FOWT models.

Test case	Model	Wind condition [m/s]	Control	Wave characteristics	Length [min]
4.1	Softwind	18, TI = 17%	DTU Controller	Hs = 5.8 m, Tp = 11 s, Bretschneider	60
4.1	OC5	12.91, TI = 5%	pitch = 1° rotor speed = 12.1 min <sup>-1</sup>	Hs = 7.1 m, Tp = 12.1 s, JONSWAP	176
4.1	Hexafloat	7.0, TI = 32.6%	ROSCO v. 2.4.1	Hs = 6.0 m, Tp = 12.0 s, JONSWAP	20

a slightly closer agreement with the experiment in the surge response compared to QBlade, which only slightly underestimates the surge amplitude. This is unsurprising as the SIL experiment and OpenFAST both utilize the same aerodynamic models.

540 The aerodynamic thrust combined with the mean drift force causes a mean surge displacement around 0.5 m that is accurately reflected in both numerical tools. The mean pitch angle enforced by the thrust force amounts to approximately 2°. The pitch response is very similar in the both numerical tools showing good alignment with the experiment. As a result, the tower base moment is in good alignment too, indicating that the aerodynamic thrust predicted by the LLFVW method is similar to the one of the SIL-experiment (AeroDyn v14) also in unsteady conditions. Given that the mean TSR of the test cases is 5, such

545 close agreement could be expected from Fig. 5. The observed offset in the fairlead tension to the experiment pointed out in the Softwind response to TCs 3.1 and 3.2 is reduced once aerodynamic thrust is included. The experiment validates the alignment between QBlade and OpenFAST, showing only slightly lower tensions. Regarding the dynamics, good agreement is found.

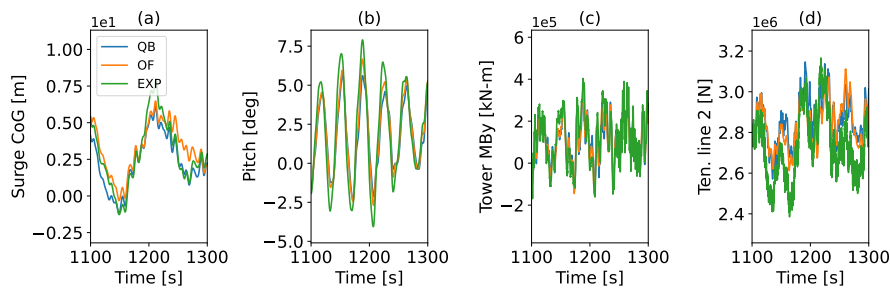


**Figure 15.** Softwind model motion and load response to TC 4.1 - combined irregular wave and wind excitation in (a) surge CoG motion, (b) pitch motion, (c) tower base fore-aft moment and (d) fairlead tension line 2.

Continuing the analysis with Fig. 16, severe response within the natural frequencies of the degrees of motion becomes evident. In fact, the response in the surge natural frequency (Fig. 16a) at around 0.01 Hz dominates the spectrum of motions to an extent that the linear wave response is only observable in the zoomed in frame due to the relative transparency of the spar-buoy type platform to linear wave excitation. In addition to the wave spectrum, the scaled wind spectrum is displayed

550





as an indicator of the excited frequencies by the turbulent wind field. The peak of the wind spectrum aligns with the peak observable at Softwind’s natural frequency. In the magnified frame, the surge response shows excellent agreement between the numerical tools and the experiment. The corresponding box-plot for the surge direction (Fig. 16e) reveals good alignment between QBlade and the experiment regarding median and IQR at -11% difference. The OpenFAST result is offset towards a larger surge displacement and yields an IQR of -16%. Figures 16b and 16h show the PSD and box-plot corresponding to the pitch DoF. The former demonstrates only minor excitation within the linear wave frequency range in contrast to a strong response in the pitch natural frequency. As continuously stated throughout this work, this excitation frequencies is matching the experiment response albeit, at a reduced scale. This leads to a slightly increased spread of the IQR of the box corresponding to the experiment compared to QBlade (-28%) and OpenFAST(-18%). The tower base moment (Figs. 16c and g), being closely related to the pitch motion of the FOWT system, matches the observations for the pitch sensor with more aligned IQRs between QBlade and OpenFAST. Excitation peaks corresponding to the natural frequencies of the coupled surge and pitch degrees of freedom can be seen in the power spectral density of the tension at the delta connection point of the Softwind platform (Figs. 16d). The box-plots of the mooring tension show yet again the consistent difference in the mooring tensions that was observed throughout the analysis of the Softwind platform.

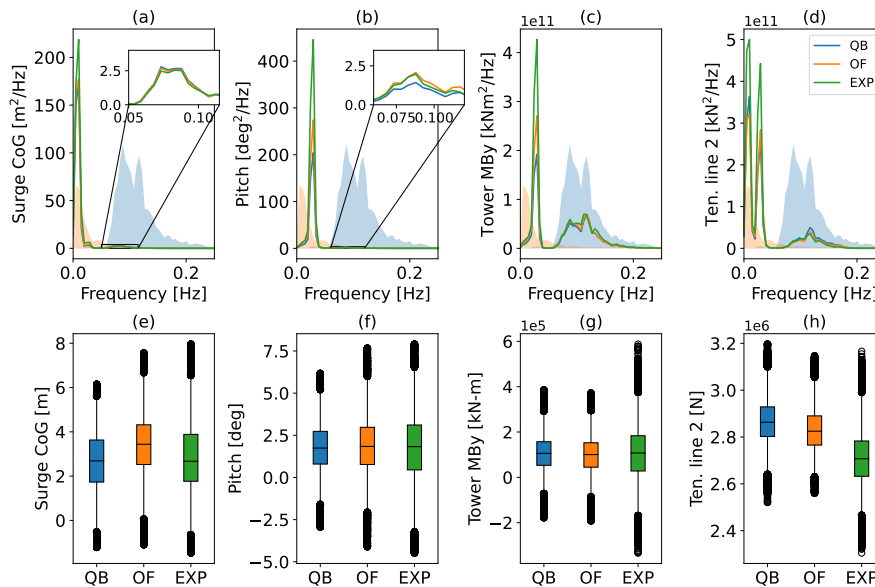


**Figure 16.** Softwind response to TC 4.1 - irregular wave and wind excitation. PSD of (a) surge CoG motion, (b) pitch motion, (c) tower base fore-aft moment, (d) fairlead tension line 2 and the corresponding box-whisker plots (e) - (h). The qualitative wave (blue) and wind (red) spectra are displayed with transparent color in the background for reference.

The corresponding PSD and box-plot of the OC5 model for TC 4.1 is shown in Fig 17. Given the fixed rotor speed of  $12.1 \text{ min}^{-1}$ , the 1P excitation frequency amounts to approximately 0.2 Hz. The PSD can still be categorized into the system’s



natural frequencies, the linear wave frequency range and the range above, which is most visible in the tower loads. Comparing to the PSD from TC 3.2 in Fig 12, an outstanding effect is the damping visible in the surge and pitch DoFs (Figs 17a and b) when aerodynamic loads are included. The aerodynamic damping comes into effect by an increased thrust force that acts on the tower top when the relative wind velocity in the rotor plan is increased during forward motion and a reduced during backwards motion. This leads to a more dampened response within the resonant frequencies of the floater. Thereby, the peak in the surge natural frequency is reduced by about 40%. In contrast, the response within the linear wave range is not changed. Furthermore, QBlade still shows a closer response to the experiment in the surge eigenfrequency peak due to the additional wave stretching model. The effect of aerodynamic damping is also seen in the box-plot (Fig 17e), where the difference in the spread of the whiskers corresponding to the experiment in surge compared to the spread seen for the numerical codes is reduced (-20% in QBlade, -23% in OpenFAST). The smaller relative difference between them within the oscillation in natural frequency leads to a closer alignment in data distribution. The same trend can be observed in the pitch PSD (Fig 17b) with a reduction of the energy within the pitch natural frequency of close to 50% compared to TC 3.2. The linear response at higher frequencies remains largely unchanged. QBlade and OpenFAST show good agreement with one another, with a slight underestimation of the linear response visible in the QBlade results. The response in the pitch natural period is underestimated by both numerical tools. Looking at Fig 17f, the relative differences in the quantile ranges between the experiment and the numerical tools are similar to the ones observed for wave-only excitation, despite the reduced relative difference in the pitch motion at low frequencies (QBlade -23%, OpenFAST -20%). QBlade shows good alignment with the median position of the experiment, while OpenFAST exhibits a slight underestimation of this position. Moving on to the tower base moment (Fig 17c), two peaks lie within the linear wave spectrum, one at 0.07 Hz aligning with the dominant wave frequency and a larger one at 0.14 Hz that doesn't. According to Robertson et al. (2017) these two peaks inside the linear wave spectrum are caused by the motion of the structure with respect to the wave. QBlade and OpenFAST capture the both peaks similarly but both underestimate the response compared to the experiment. The underestimation of the response in this frequency is in line with the participants of the OC5 collaboration that deployed a LPMD approach. Furthermore, the tower fore-aft moment PSD shows peaks in the pitch natural frequency and in the tower fore-aft natural frequency. Here, in contrast to Fig. 12, the shape of the peak predicted by QBlade aligns closely with the OC5 experiment, while OpenFAST overestimates the response at an accurate tower frequency. Good agreement in the box-plot that corresponds to the tower fore-aft moment is visible (Fig. 17g). The tension within fairlead 2 (Figs. 17d and h) reflects the increased loads on the mooring system due to the aerodynamic loads compared to TC 3.2. Good alignment is present within the linear frequency range. The increased response of the experimental model in the surge natural period is reflected again in the tension of this line. Moreover, a similar data distribution of the QBlade results compared to OpenFAST and the experiment can be seen.

The final case that is discussed in this study is the combined wind and wave excitation case for the Hexafloat model. As Table 5 lists, below-rated conditions are assumed. Consequently, the ROSCO v 2.4.1 controller follows the objective of maximizing power by adjusting rotational speed to operate at the optimal TSR of 8.06. According to Fig. 5, the aerodynamic models of DeepLines Wind<sup>TM</sup> and QBlade demonstrate close agreement with regards to the thrust coefficient in this condition. Hence, similar response on the motion DoFs and loads are to be expected with similarly behaving hydrodynamic models. A time

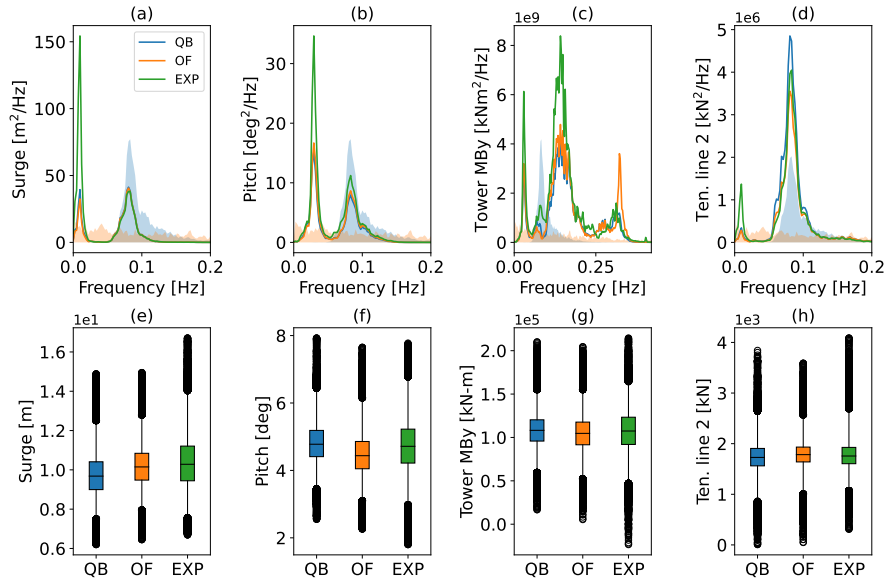


**Figure 17.** OC5 model response to TC 4.1 - irregular wave and wind excitation. PSD of (a) surge motion, (b) pitch motion, (c) tower base fore-aft moment, (d) fairlead tension line 2 and the corresponding box-whisker plots (e) - (h). The qualitative wave (blue) and wind (red) spectra are displayed with transparent color in the background for reference.

series comparison of the motion and load sensors (not shown here for brevity) confirms this with very good agreement between both simulation tools in the surge and pitch degrees of freedom. In the platform pitch response, QBlade demonstrates slightly  
 605 increased amplitudes in frequencies that appeared to be within the linear frequency range of the wave field.

The PSDs in Fig. 18 are dominated by the resonant response in the natural surge and pitch frequencies. The response within the linear frequency range only becomes visible within the magnified cut-outs, where good alignment in the time series is confirmed. In contrast to the other two FOWT models that rely on a LPMD approach, the buoyancy calculation at the instantaneous position and submerged volume combined with the MacCamy-Fuchs correction is modeling the wave excitation in this  
 610 Morison representation. The box-plots show a closely matched distribution of the data, with the most prominent difference being visible in the surge DoF and in the 99% quantile of the fairlead tension in line 2 (Fig. 18e and h). This however is not caused by hydrodynamic treatment but due to the coupled effects that the servo-dynamics have on the overall response of the turbine, as will be discussed next.

The small deviation described above in the floater pitch response can partially be traced back to the rotational speed that is  
 615 controlled by the ROSCO controller. Figure 19 displays for reference the floater pitch along with the rotational speed which contains a high frequency component in the QBlade results that is not captured in DeepLines Wind<sup>TM</sup> (Figs. 19a and b). As a result of the small spikes visible in the rotational speed time series, the thrust force will follow this behavior in QBlade and thus cause the slightly increased pitch motion of the floating platform. Following the causal chain further, this deviation is visible in the generator torque (Fig. 19c), where DeepLines Wind<sup>TM</sup> predicts a calmer torque control response compared

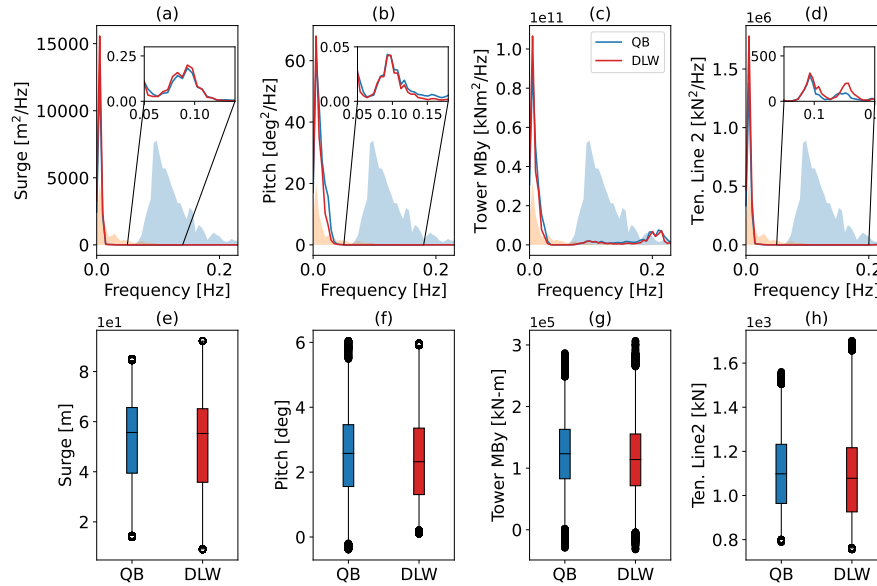


**Figure 18.** Hexafloat model response to TC 4.1 - irregular wave and wind excitation. PSD of (a) surge cog motion, (b) pitch motion, (c) tower base fore-aft moment, (d) fairlead tension line 2 and the corresponding box-whisker plots (e) - (h). The qualitative wave (blue) and wind (red) spectra are displayed with transparent color in the background for reference.

620 to QBlade. Since the turbine is operating at below-rated condition, the blade pitch is only activated temporarily when the rotor speed briefly exceeds rated speed. One example of this can be seen at 1350 s of simulation time, where the increase in rotor speed causes the controller to pitch blades (Fig. 19d). The controller response in QBlade is more dynamic, and it triggers the controller to activate the blade pitch at a few, much shorter torque spikes. Even though the differences in drive train dynamics and the following pitch controller actuation seem to have only minor influence on overall dynamics, this picture changes drastically when the FOWT is operating in regimes with above-rated wind speed. Figure 20 shows an example of this. The turbulent wind in this figure contains velocities above-rated between 700 s and 1100 s. Here, the rotational speed once again fluctuates more in QBlade compared to DeepLines Wind<sup>TM</sup> and this leads to larger blade pitch actuation (Figs. 20a and b). The drastic influence on system dynamics is visible in the surge and pitch DoFs. The QBlade model undergoes much larger oscillations with amplitudes of 5.5 m in surge and 4.5 deg in pitch compared 1.5 m and 1.2 deg in DeepLines Wind<sup>TM</sup>.  
 625  
 630 When the wind speed dips below-rated and the blade pitch actuation is not required (above 1100 s), the platform surge and pitch responses quickly align (Figs. 19c and d). We have not yet fully understood the large differences seen for this model when above-rated conditions are present. Especially, given the accuracy of the QBlade results compared to OpenFAST and the Softwind experiment at above-rated conditions, which also include a controller. Further research must be carried out to better understand this phenomenon and isolate whether it emerges from differences between QBlade and DeepLines Wind<sup>TM</sup> in the  
 635 aerodynamic treatment or the controller interface.

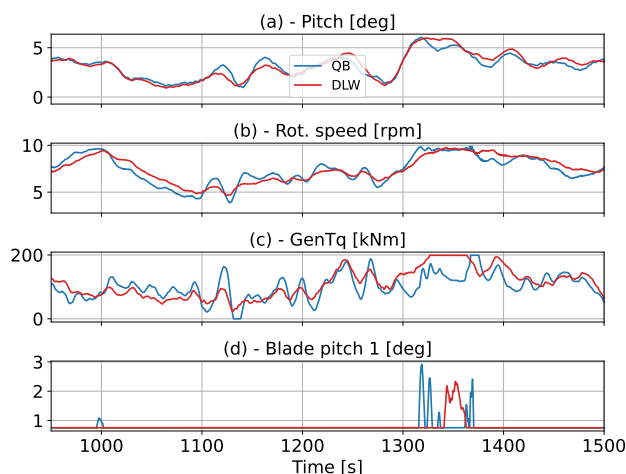


**Figure 19.** Hexafloat model controller actuation (ROSCO 2.4.1) - combined irregular wave and wind excitation: (a) platform pitch, (b) rotor speed, (c) generator torque (high speed shaft) and (d) blade pitch.

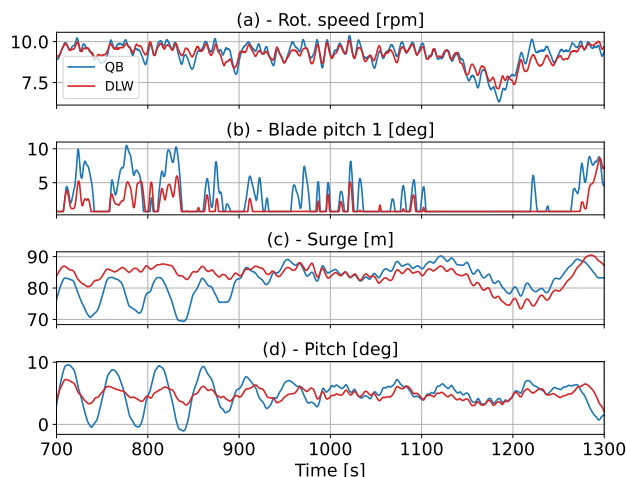


**Figure 20.** Hexafloat model controller actuation and motion response - combined irregular wave and wind excitation: (a) rotor speed, (b) blade pitch, (c) platform surge and (d) platform pitch . Wind with 11.4 m/s, 15 % TI and wave field with JONSWAP spectrum with  $H = 7.7$  m and  $T = 12.4$  s.

## 5 Conclusion and Outlook

In this work, the hydrodynamic module QBlade-Ocean, developed to expand the capabilities of the wind turbine simulation tool QBlade for offshore simulations, is verified and validated on three floating offshore wind turbine models. The three models encompass a variety of different substructure concepts. They are the semi-submersible OC5 FOWT (5MW MSWT on the DeepCWind structure), the Softwind FOWT (DTU 10 MW RWT on a spar-buoy type platform called Softwind) and the



Hexafloat (DTU 10 MW RWT on the Hexafloat substructure). In case of the former two, an experimental campaign was used to validate the results produced within QBlade. Furthermore, equivalent models were built in OpenFAST to verify the results with a state-of-the-art code. In case of the Hexafloat model, a code-to-code comparison with the simulation tool DeepLines Wind<sup>TM</sup> was carried out as no experimental data was available. The OC5 and Softwind models were simulated using linear potential flow theory combined with Morison drag, whereas the Hexafloat model was simulated using a strip theory based full Morison approach.

The validation and verification cases ranged from simplified test cases up to fully coupled aero-hydro-servo-elastic simulations with irregular wave and wind excitation. The simplified cases were selected to confirm a correct model definition. In these cases, the neutral position, the mooring system, the relevant natural frequencies as well as the aerodynamic performance of the rotor on a constrained platform were analyzed. On the one hand, these tests helped to validate and verify some of the newly implemented functionality such as the buoyancy and mooring modules in static conditions. On the other hand, the model definitions themselves were confirmed and uncertainties stemming from using different aero-elastic modules could be estimated. The complexity of the test cases gradually increased thereafter with cases that omitted the influence of aerodynamics and solely excited the FOWTs with regular and irregular wave fields. The final case analyzed the fully coupled system of a floating offshore wind turbine with irregular waves, turbulent wind and a full supervisory wind turbine controller.

In the decay tests, both QBlade and OpenFAST recreated the experimental results, thus validating the implementation of the radiation forces and Morison drag. As is common practice, both tools required minor tuning of damping and stiffness parameters to fully align with the reference. Uncertainties in the model specification of the experiments are one reason for this. OpenFAST showed a tendency to overpredicted the length of the surge natural periods of both, the OC5 and Softwind models, compared to the QBlade model and the experiment. DeepLines Wind<sup>TM</sup> and QBlade showed close to perfect alignment throughout all degrees of freedom in the decay tests on the Hexafloat.

Regular wave excitation cases validated the implementation of diffraction effects and Froud-Krylov forces. In QBlade they can be modeled either through linear potential flow theory (OC5 and Softwind) or through the use of the full Morison equation with the MacCamy-Fuchs correction combined with explicitly calculating the buoyancy based on the instantaneous submerged volume (Hexafloat). The RAOs in relation to the reference (experiments for OC5 and Softwind) and to DeepLines Wind<sup>TM</sup> (for the Hexafloat) validated and verified both approaches in QBlade. The deviation to the experiments were comparable to those of OpenFAST and amounted to less than 3% in surge, 6% in heave and 12% in pitch, where amplitudes are minor and thus cause large relative differences for small absolute values. Moreover, the spectral analysis of the models responses showed excitation of the tower structure natural frequencies outside of the frequency of the regular wave. This highlights the importance of importing identical wave elevation data to experimental campaigns for such comparisons.

In the next step, QBlade's ability to capture non-linear excitation and more complex system dynamics was verified with irregular wave excitation. For the FOWTs modeled with LPMD, sum- and difference frequency quadratic transfer functions (OC5) and Newman's approximation (Softwind) were applied to capture the mean drift and non-linear forces. For the full Morison treatment, weak, non-linear excitation was calculated through the application of hydrodynamic loads at the instantaneous position. Wheeler stretching was employed for each model in QBlade. The analysis in the spectral space confirmed the



observations made throughout the OC5 and OC6 collaborations; Non-linear excitation frequencies were captured accurately but with a considerably dampened response compared to experiments. As stated by Robertson et al. (2020) and Robertson and Wang (2021) the tuning process might be part of the reason for this. Wheeler stretching led to a 6% improvement compared to OpenFAST with respect to the OC5 experiment in the surge direction. The Softwind platform showed discrepancies in mooring  
680 tensions between numerical codes and the experiment. QBlade and OpenFAST overestimated the loads by 6.3% and 5% respectively. These discrepancies potentially could be attributed to uncertainties in the description of the experimental setup and the required tuning to match the system characteristics of the experiment. Nonetheless, the analysis of the PSDs yielded similar responses between QBlade, OpenFAST and the experiment for platform motions and loads. The comparison to DeepLines Wind<sup>TM</sup>, based on the Hexafloat model, showed good accordance in the frequency domain, with modestly increased energy  
685 within the several peaks predicted by QBlade. In terms of interquartile ranges this led to an increase of the spread by 14% in surge and 19% in pitch motions.

The final test case validated and verified the fully coupled aero-hydro-servo-elastic response predicted by QBlade for the three FOWTs. The discrepancy within the non-linear excitation in the natural frequencies of the LPMD models continued to stand out. However, due to aerodynamic damping, with reduced difference regarding the experimental campaigns. Otherwise,  
690 the qualitative and quantitative analysis of the QBlade results yielded steadily comparable results to OpenFAST with partially closer agreement to the experiments, due to some advanced capabilities such as kinematic stretching, increased aerodynamic fidelity and explicit buoyancy calculation. A 3 and 5 percentage point improvement in the surge interquartile range was seen for the OC5 and Softwind models respectively. The code-to-code comparison on the Hexafloat demonstrated the influence of minor differences in the controller actuation to the overall system dynamics. It was found that the combination of an  
695 extremely slack mooring system, a minor increase in the motion response to the linear wave spectrum in QBlade and a more inert behavior of the drive train dynamics in DeepLines Wind<sup>TM</sup> led to differences in the dynamics of platform pitch. These differences between QBlade and DeepLines Wind<sup>TM</sup> were vastly amplified when operating conditions above-rated wind speed were analyzed. Here, amplitudes in the substructure pitch oscillations up to 4.5 degrees were seen in QBlade compared to 1.2 degrees in DeepLines Wind<sup>TM</sup>.

700 Concluding this study, the openly available simulation suite QBlade was expanded by a hydrodynamic module called QBlade-Ocean. This module addresses a need for accurate and fast simulation tools that enable more competitive FOWT designs. The flexible framework of QBlade allows the combination of different modeling approaches. The LPMD and full Morison approaches were validated with two experimental campaigns and verified against the state-of-the-art simulation tools OpenFAST and DeepLines Wind<sup>TM</sup>. The results of QBlade-Ocean showed good agreement with both tools and the experimental  
705 results. Differences that were seen mostly related to the application of distinct aerodynamic and structural models. In the case of QBlade, these models were validated in previous studies. Since a floating offshore wind turbine is a complex, tightly coupled multi-disciplinary system, differences in the modeling approaches will influence the overall dynamics and loads of the system. It was already shown in this study that differences in aero-servo-dynamic modeling can cause significant deviation in the overall dynamic system response of the Hexafloat model.



710 Work conducted concurrently with this study included a quantitative analysis to determine the effects of using more accurate modeling approaches, such as the LLFVW aerodynamic solver, in FOWT simulations on damage equivalent loads under realistic environmental conditions. This is an important step towards a possible improvement of future FOWT designs. As part of the FLOATECH project, a paper focusing on this matter has been submitted recently (Papi et al., 2023). Future work will focus on the integration of QBlade with optimization algorithms, where the increased fidelity in the structural and aerodynamic methods could be leveraged to facilitate the development of more accurate surrogate models, which in turn can be included efficiently in optimization problems.

## Nomenclature

**BEM** Blade Element Momentum Theory

**DoF** Degree of Freedom

720 **FEA** Finite Element Analysis

**FOWT** Floating Offshore Wind Turbine

**GUI** Graphical User Interface

**LLFVW** Lifting Line Free Vortex Wake

**LPMD** Liner Potential Flow approach with the addition of Morison Drag

725 **MARIN** Maritime Research Institute Netherlands

**MSWT** MARIN Stock Wind Turbine

**NREL** National Renewable Energy Laboratory

**QTF** Quadratic Transfer Function

**PSD** Power Spectral Density


730 **SIL** Software-In-the-Loop

**TSR** Tip Speed Ratio

**TUB** Technische Universität Berlin





*Acknowledgements.*  This work has received funding from the European Union's Horizon 2020 research and innovation programme  
735 under grant agreement No 101007142

*Code and data availability.* The three QBlade models that are used in this study can be accessed under the following DOIs: i) OC5 10.5281/zenodo.7037223 ii) Softwind 10.5281/zenodo.7821271. iii) Hexafloat 10.5281/zenodo.7037256.

*Author contributions.* All authors contributed to this work. In particular, the numerical models in QBlade, OpenFAST and DeepLines Wind<sup>th</sup> were built and simulated by the groups at TUB, University of Florence and Marie-Laure Ducasse, respectively. Felicién Bonnefoy provided  
740 the necessary information to accurately build and tune the Softwind FOWT and offered consultation on the interpretation of the corresponding experimental results.

*Competing interests.* At least one of the (co-)authors is a member of the editorial board of Wind Energy Science.



## References

- Arnal, V.: Experimental Modelling of a floating wind turbine using a "software-in-the-loop" approach, Ph.D. thesis, 2020.
- 745 Babarit, A. and Delhommeau, G.: Theoretical and numerical aspects of the open source BEM solver NEMOH, 11th European Wave and Tidal Energy Conference (EWTEC2015), 2015.
- Bak, C., Zahle, F., Bitsche, R., Kim, T., Yde, A., Henriksen, L., Natarajan, A., and Hansen, M.: Description of the DTU 10 MW Reference Wind Turbine, DTU Wind Energy Report-I-0092, 2013.
- Behrens de Luna, R., Marten, D., Barlas, T., Horcas, S. G., Ramos-García, N., Li, A., and Paschereit, C. O.: Comparison of different fidelity aerodynamic solvers on the IEA 10 MW turbine including novel tip extension geometries, *Journal of Physics: Conference Series*, 2265, 032 002, <https://doi.org/10.1088/1742-6596/2265/3/032002>, 2022.
- 750 Burton, T., Sharpe, D., Jenkins, N., and Bossanyi, E.: *Wind Energy Handbook*, John Wiley & Sons, <https://books.google.de/books?id=4UYm893y-34C>, 2001.
- Deperrois, A.: XFLR5 Website, <http://www.xflr5.tech/xflr5.htm>, last accessed on 14.08.2023.
- 755 Drela, M.: XFOIL: An Analysis and Design System for Low Reynolds Number Airfoils, vol. 54, [https://doi.org/10.1007/978-3-642-84010-4\\_1](https://doi.org/10.1007/978-3-642-84010-4_1), 1989.
- ElastoDyn: Online documentation, <https://openfast.readthedocs.io/en/dev/source/user/elastodyn/index.html>, last accessed on 14.08.2023.
- FLOATECH: Project Website, <https://www.floatech-project.com/>, last accessed on 23.08.2023, 2020.
- Goupee, A., Kimball, R., Ridder, E.-J., Helder, J., Robertson, A., and Jonkman, J.: A calibrated blade-element/momentum theory aerodynamic model of the MARIN stock wind turbine, 2015, 584–592, 2015.
- 760 Hansen, M. H. and Henriksen, L. C.: Basic DTU Wind Energy controller, no. 0028 in DTU Wind Energy E, DTU Wind Energy, Denmark, 2013.
- HydroDyn: Online documentation, <https://openfast.readthedocs.io/en/dev/source/user/hydrodyn/index.html>, last accessed on 14.08.2023.
- Jeon, M., Lee, S., and Lee, S.: Unsteady aerodynamics of offshore floating wind turbines in platform pitching motion using vortex lattice method, *Renewable Energy*, 65, 207–212, <https://doi.org/10.1016/j.renene.2013.09.009>, 2014.
- 765 Jonkman, B., Buhl, M., and Jonkman, J.: OpenFAST GitHub Repository, <https://github.com/old-NWTC/FAST>, 2019.
- Jonkman, J.: Definition of the Floating System for Phase IV of OC3, NREL technical report, <https://doi.org/10.2172/979456>, 2010.
- Jonkman, J., Jonkman, B., and Dimiani, R.: AeroDyn v14, <https://github.com/OpenFAST/openfast/tree/main/modules/aerodyn>, last accessed on 06.09.2023.
- 770 Jonkman, J. M. and Buhl, Jr, M. L.: FAST User's Guide - Updated August 2005, <https://doi.org/10.2172/15020796>, 2005.
- Kurnia, R. and Ducrozet, G.: NEMOH: Open-source boundary element solver for computation of first- and second-order hydrodynamic loads in the frequency domain, *Computer Physics Communications*, 292, 108 885, <https://doi.org/https://doi.org/10.1016/j.cpc.2023.108885>, 2023.
- Larsen, T. and Hansen, A.: How 2 HAWC2, the user's manual, no. 1597(ver. 3-1)(EN) in Denmark. Forskningscenter Risoe. Risoe-R, Risø National Laboratory, 2007.
- 775 Li, A., Pirrung, G. R., Gaunaa, M., Madsen, H. A., and Horcas, S. G.: A computationally efficient engineering aerodynamic model for swept wind turbine blades, *Wind Energy Science*, 7, 129–160, <https://doi.org/10.5194/wes-7-129-2022>, 2022.
- Madsen, H. A., Larsen, T. J., Pirrung, G. R., Li, A., and Zahle, F.: Implementation of the blade element momentum model on a polar grid and its aeroelastic load impact, *Wind Energy Science*, 5, 1–27, <https://doi.org/10.5194/wes-5-1-2020>, 2020.



- 780 Mancini, S., Boorsma, K., Schepers, G., and Savenije, F.: A comparison of dynamic inflow models for the blade element momentum method, *Wind Energy Science*, 8, 193–210, <https://doi.org/10.5194/wes-8-193-2023>, 2023.
- Marten, D.: QBlade: A Modern Tool for the Aeroelastic Simulation of Wind Turbines, Ph.D. thesis, <https://doi.org/10.14279/depositonce-10646>, 2020.
- Murray, R., Hayman, G., Jonkman, J., and Damiani, R.: AeroDyn V15.04: Design Tool for Wind and MHK Turbines, Tech. rep.,  
785 <https://doi.org/10.15473/1415580>, 2017.
- NREL: ROSCO. Version 2.4.1, <https://github.com/NREL/ROSCO>, last accessed on 06.09.2023, 2021.
- OpenFAST Documentation: <https://openfast.readthedocs.io/en/dev/index.html>, last accessed on 07.09.2023, 2023.
- Papi, F., Troise, G., Behrens de Luna, R., Saverin, J., Perez-Becker, S., Marten, D., Ducasse, M.-L., and Bianchini, A.: A Code-to-Code  
Comparison for Floating Offshore Wind Turbine Simulation in Realistic Environmental Conditions: Quantifying the Impact of Modeling  
790 Fidelity on Different Substructure Concepts, *Wind Energy Science Discussions*, 2023, 1–34, <https://doi.org/10.5194/wes-2023-107>, 2023.
- Perdrizet, T., Gilloteaux, J.-C., Teixeira, D., Ferrer, G., Piriou, L., Cadiou, D., Heurtier, J.-M., and Le Cunff, C.: Fully Coupled Floating Wind  
Turbine Simulator Based on Nonlinear Finite Element Method: Part II — Validation Results, vol. Volume 8: Ocean Renewable Energy of  
*International Conference on Offshore Mechanics and Arctic Engineering*, p. V008T09A052, <https://doi.org/10.1115/OMAE2013-10785>,  
2013.
- 795 Perez-Becker, S. and Behrens de Luna, R.: Aero-Hydro-Elastic Model Definition in QBlade-Ocean, Tech. rep.,  
<https://doi.org/10.5281/zenodo.6958204>, 2022.
- Perez-Becker, S., Papi, F., Saverin, J., Marten, D., Bianchini, A., and Paschereit, C. O.: Is the Blade Element Momentum theory overesti-  
mating wind turbine loads? – An aeroelastic comparison between OpenFAST’s AeroDyn and QBlade’s Lifting-Line Free Vortex Wake  
method, *Wind Energy Science*, 5, 721–743, <https://doi.org/10.5194/wes-5-721-2020>, 2020.
- 800 Perez-Becker, S., Saverin, J., Behrens de Luna, R., Papi, F., Combreau, C., Ducasse, M.-L., Marten, D., and Bianchini, A.: Validation Report  
of QBlade-Ocean, Tech. rep., <https://doi.org/10.5281/zenodo.7817605>, 2022.
- Principia: Company website, <https://www.principia-group.com/blog/product/deeplines-wind/>, last accessed on 23.08.2023.
- QBlade Documentation: <https://docs.qblade.org/>, last accessed on 23.08.2023, 2022.
- Ramos-García, N., Kontos, S., Pegalajar-Jurado, A., González Horcas, S., and Bredmose, H.: Investigation of the floating IEA Wind 15 MW  
805 RWT using vortex methods Part I: Flow regimes and wake recovery, *Wind Energy*, 25, 468–504, <https://doi.org/10.1002/we.2682>, 2022.
- Rinker, J., Gaertner, E., Zahle, F., Skrzypiński, W., Abbas, N., Bredmose, H., Barter, G., and Dykes, K.: Comparison of loads from  
HAWC2 and OpenFAST for the IEA Wind 15 MW Reference Wind Turbine, *Journal of Physics: Conference Series*, 1618, 052052,  
<https://doi.org/10.1088/1742-6596/1618/5/052052>, 2020.
- Roald, L., Jonkman, J., Robertson, A., and Chokani, N.: The Effect of Second-order Hydrodynamics on Floating Offshore Wind Turbines,  
810 *Energy Procedia*, 35, 253–264, <https://doi.org/https://doi.org/10.1016/j.egypro.2013.07.178>, deepWind’2013 – Selected papers from 10th  
Deep Sea Offshore Wind RD Conference, Trondheim, Norway, 24 – 25 January 2013, 2013.
- Robertson, A.: Uncertainty Analysis of OC5-DeepCwind Floating Semisubmersible Offshore Wind Test Campaign, [https://www.osti.gov/  
biblio/1416717](https://www.osti.gov/biblio/1416717), 2017.
- Robertson, A.: IEA Wind TCP Task 30 (OC6), <https://iea-wind.org/task30/>, last accessed on 25.08.2023, 2019.
- 815 Robertson, A. and Wang, L.: OC6 Phase Ib: Floating Wind Component Experiment for Difference-Frequency Hydrodynamic Load Valida-  
tion, *Energies*, 14, 6417, <https://doi.org/10.3390/en14196417>, 2021.



- Robertson, A., Jonkman, J., Wendt, F., Goupee, A., and Dagher, H.: Definition of the OC5 Deep-Cwind Semisubmersible Floating System, <https://a2e.energy.gov/api/datasets/oc5/oc5.phase2/files/oc5.phase2.model.definition-semisubmersible-floating-system-phase2-oc5-ver15.pdf>, 2014.
- 820 Robertson, A., Wendt, F., Jonkman, J., Popko, W., Dagher, H., Gueydon, S., Qvist, J., Vittori, F., Azcona, J., Uzunoglu, E., Guedes Soares, C., Harries, R., Yde, A., Galinos, C., Hermans, K., Bernardus de Vaal, J., Bozonnet, P., Bouy, L., Bayati, I., Bergua, R., Galvan, J., Mendikoa, I., Barrera Sanchez, C., Shin, H., Oh, S., Molins, C., and Debruyne, Y.: OC5 Project Phase II: Validation of Global Loads of the DeepCwind Floating Semisubmersible Wind Turbine, *Energy Procedia*, 137, 38–57, <https://doi.org/https://doi.org/10.1016/j.egypro.2017.10.333>, 14th Deep Sea Offshore Wind RD Conference, EERA DeepWind'2017, 2017.
- 825 Robertson, A., Gueydon, S., Bachynski, E., Wang, L., Jonkman, J., Alarcón, D., Amet, E., Beardsell, A., Bonnet, P., Boudet, B., Brun, C., Chen, Z., Féron, M., Forbush, D., Galinos, C., Galvan, J., Gilbert, P., Gómez, J., Harnois, V., Haudin, F., Hu, Z., Dreff, J. L., Leimeister, M., Lemmer, F., Li, H., Mckinnon, G., Mendikoa, I., Moghtadaei, A., Netzband, S., Oh, S., Pegalajar-Jurado, A., Nguyen, M. Q., Ruehl, K., Schünemann, P., Shi, W., Shin, H., Si, Y., Surmont, F., Trubat, P., Qvist, J., and Wohlfahrt-Laymann, S.: OC6 Phase I: Investigating the underprediction of low-frequency hydrodynamic loads and responses of a floating wind turbine, *Journal of Physics: Conference Series*, 830, 1618, 032 033, <https://doi.org/10.1088/1742-6596/1618/3/032033>, 2020.
- Saverin, J., Perez-Becker, S., Behrens de Luna, R., Marten, D., Gilloteaux, J.-C., and Kurnia, R.: Higher Order Hydroelastic Module, Tech. rep., <https://doi.org/10.5281/zenodo.6958081>, 2021.
- Shaler, K., Branlard, E., and Platt, A.: OLAF User's Guide and Theory Manual, Tech. Rep. NREL/TP-5000-75959, 1659853, MainId:6799, <https://doi.org/10.2172/1659853>, 2020.
- 835 Tasora, A., Serban, R., Mazhar, H., Pazouki, A., Melanz, D., Fleischmann, J., Taylor, M., Sugiyama, H., and Negrut, D.: Chrono: An Open Source Multi-physics Dynamics Engine, in: *Lecture Notes in Computer Science*, pp. 19–49, Springer International Publishing, [https://doi.org/10.1007/978-3-319-40361-8\\_2](https://doi.org/10.1007/978-3-319-40361-8_2), 2016.
- van Garrel, A.: Development of a Wind Turbine Aerodynamics Simulation Module, Tech. rep., <https://doi.org/10.13140/RG.2.1.2773.8000>, 2003.
- 840 Veers, P., Dykes, K., Lantz, E., Barth, S., Bottasso, C. L., Carlson, O., Clifton, A., Green, J., Green, P., Holttinen, H., Laird, D., Lehtomäki, V., Lundquist, J. K., Manwell, J., Marquis, M., Meneveau, C., Moriarty, P., Munduate, X., Muskulus, M., Naughton, J., Pao, L., Paquette, J., Peinke, J., Robertson, A., Sanz Rodrigo, J., Sempreviva, A. M., Smith, J. C., Tuohy, A., and Wisser, R.: Grand challenges in the science of wind energy, *Science*, 366, eaau2027, <https://doi.org/10.1126/science.aau2027>, 2019.
- WAMIT Inc.: Wamit User Manual, Version 7.4, Chestnut Hill, MA 02467-2504, USA.
- 845 Wendt, F., Robertson, A., Jonkman, J., and Andersen, M. T.: Verification and Validation of the New Dynamic Mooring Modules Available in FAST v8: Preprint, <https://www.osti.gov/biblio/1295390>, 2016.
- Yu, W., Müller, K., and Lemmer, F.: Qualification of innovative floating substructures for 10MW wind turbines and water depths greater than 50m, Tech. rep., LIFES50+, 2018.